AFRL-RV-PS-
TR-2012-0228

ASSESSMENT OF REGIONAL EXPLOSION DISCRIMINANTS USING DATA SETS OF UNPARALLELED SPATIAL SAMPLING

Kate C. Miller, et al.

Texas A&M University
College of Geosciences
MS3148 TAMU
College Station, TX 77843-3148

31 October 2012

Final Report

AIR FORCE RESEARCH LABORATORY
Space Vehicles Directorate
3550 Aberdeen Ave SE
AIR FORCE MATERIEL COMMAND
KIRTLAND AIR FORCE BASE, NM 87117-5776

DTIC COPY

NOTICE AND SIGNATURE PAGE

This report was cleared for public release by the 377 ABW Public Affairs Office and is available to the general public, including foreign nationals. Copies may be obtained from the Defense Technical Information Center (DTIC) (http://www.dtic.mil).

AFRL-RV-PS-TR-2012-0228 HAS BEEN REVIEWED AND IS APPROVED FOR PUBLICATION IN ACCORDANCE WITH ASSIGNED DISTRIBUTION STATEMENT.

//SIGNED//	//SIGNED//
Robert Raistrick	Edward J. Masterson, Colonel, USAF
Project Manager, AFRL/RVBYE	Chief, Battlespace Environment Division

REPORT DOCUMENTATION PAGE

Form Approved
OMB No. 0704-0188

1. REPORT DATE *(DD-MM-YY)*	**2. REPORT TYPE**	**3. DATES COVERED** *(From - To)*
31-10-2012	Final Report	07 May 2010 – 30 September 2012

4. TITLE AND SUBTITLE
Assessment of Regional Explosion Discriminants Using Data Sets of Unparalleled Spatial Sampling

5a. CONTRACT NUMBER
FA9453-10-C-0214

5b. GRANT NUMBER

5c. PROGRAM ELEMENT NUMBER
62601F

6. AUTHOR(S)
Kate C. Miller, Lindsay L. Worthington, Steven Harder, Scott Phillips, Hans Hartse, and Anne F. Sheehan

5d. PROJECT NUMBER
1010

5e. TASK NUMBER
PPM00005452

5f. WORK UNIT NUMBER
EF004085

7. PERFORMING ORGANIZATION NAME(S) AND ADDRESS(ES)
Texas A&M University
College of Geosciences
MS3148 TAMU
College Station, TX 77843-3148

8. PERFORMING ORGANIZATION REPORT NUMBER

9. SPONSORING / MONITORING AGENCY NAME(S) AND ADDRESS(ES)
Air Force Research Laboratory
Space Vehicles Directorate
3550 Aberdeen Ave SE
Kirtland AFB, NM 87117-5776

10. SPONSOR/MONITOR'S ACRONYM(S)
AFRL/RVBYE

11. SPONSOR/MONITOR'S REPORT NUMBER(S)
AFRL-RV-PS-TR-2012-0228

12. DISTRIBUTION / AVAILABILITY STATEMENT
Approved for public release; distribution is unlimited. (377ABW-2013-0028 dtd 09 Jan 2013)

13. SUPPLEMENTARY NOTES

14. ABSTRACT
We used data from the Bighorn Arch Seismic Experiment (BASE) to determine P-wave velocity structure and assess regional explosion discriminants in north-central Wyoming. BASE is a multi-scale, hybrid active/passive seismic experiment designed to determine crust and mantle structure below the Bighorn Mountains. North-central Wyoming experiences a spectrum of manmade and natural events, from regional earthquakes and teleseisms to mine blasts and single fire shots, making the region a compelling natural laboratory in which to investigate implications for regional discrimination. The velocity structure across the region is calculated through tomographic inversion of arrival times from 21 controlled-source single-fired seismic shots. The detailed velocity models can also be used to investigate the degree of spatial sampling of the seismic wavefield needed to characterize 3D wave propagation effects. For the discrimination study, we used the single-charge explosions from the BASE experiment, mining explosions, and ~40 earthquakes to test seismic discriminants using USARRAY broadband data and data recorded at station RSSD. An amplitude ratio of Pg (6-12 Hz) versus Lg (6-12 Hz) mostly separated the earthquakes from the explosions. Lg spectral ratios also separated the explosions from the earthquakes, but not as well as the Pg/Lg ratio.

15. SUBJECT TERMS:
AFRL, discrimination, seismic tomography

16. SECURITY CLASSIFICATION OF:			**17. LIMITATION OF ABSTRACT**	**18. NUMBER OF PAGES**	**19a. NAME OF RESPONSIBLE PERSON**
a. REPORT	**b. ABSTRACT**	**c. THIS PAGE**			Robert Raistrick
Unclassified	Unclassified	Unclassified	Unlimited	46	**19b. TELEPHONE NUMBER** *(include area code)*

Standard Form 298 (Rev. 8-98)
Prescribed by ANSI Std. 239.18

This page is intentionally left blank.

Table of Contents

List of Figures

1. INTRODUCTION

Discrimination of regional earthquakes, single-fired explosions and delay-fired mining explosions is dependent upon separation of path and source. The primary objective for this work is to investigate the degree of spatial sampling of the seismic wavefield and characterization of the 3D wave propagation effects that is necessary in a complex regional setting to fully assess the performance of regional seismic discriminants as they are applied to earthquakes, contained single-fired explosions, delay-fired mining explosions and mining collapses. This result will provide a basis for assessing regional discrimination performance in areas with comparatively sparse data sets.

The work for this contract is integrated with the Bighorns Arch Seismic Experiment (BASE), a project sponsored by the National Science Foundation EarthScope program. The focus of BASE is imaging the deep structure of basement-cored arches in order to understand the mechanisms of the formation of the Rocky Mountains. Other BASE science goals are focused on the nature of faults at depth in the crust and deep crustal rheology. In addition to producing velocity models of the crust and upper mantle, the seismic imaging experiment will determine whether faults at depth remain discrete or if they diffuse into a broader zone of ductile deformation.

During 2009-2010, we collected a large and diverse seismic data set in north-central Wyoming as part of BASE (Figure 1). BASE consists of a hybrid active/passive short-term seismic deployment that greatly increases the spatial sampling of the seismic wavefield in north central Wyoming, a region with abundant natural and man-made events. The BASE deployment consisted of five components. The first was a ~1 yr deployment of 39 broadband systems to infill the NSF-EarthScope USArray Transportable Array in the vicinity of the Big Horn Mountains to achieve an average spacing of 35 km. The second is an array of 170 short-period instruments deployed along a grid of five lines with a station spacing of 5 to 10 km. The third component consisted of three 5-element regional seismic arrays deployed to assess the role of arrays in signal detection and characterization for discrimination purposes. These arrays were in place for 6 months, beginning in May 2010. In July 2010, an active source seismic experiment consisting of two profiles with 1850 "Texan" seismographs deployed at 0.1 to 0.5 km and up to 20 large (500-2000 lb.) single-fired shots was conducted. The seismic signals from the shots were also recorded by the passive arrays. Finally, 850 Texan seismographs were deployed for two weeks along the short-period grid in passive mode to achieve a nominal station spacing of 1 km.

This report consists of two primary components undertaken by the PI's and collaborators:

1. An analysis of two active-source wide-angle reflection and refraction profiles across the Bighorn Mountains and the Bighorn and Powder River Basins (Figure 1). We have developed compressional wave velocity models through a series of tomographic inversions.

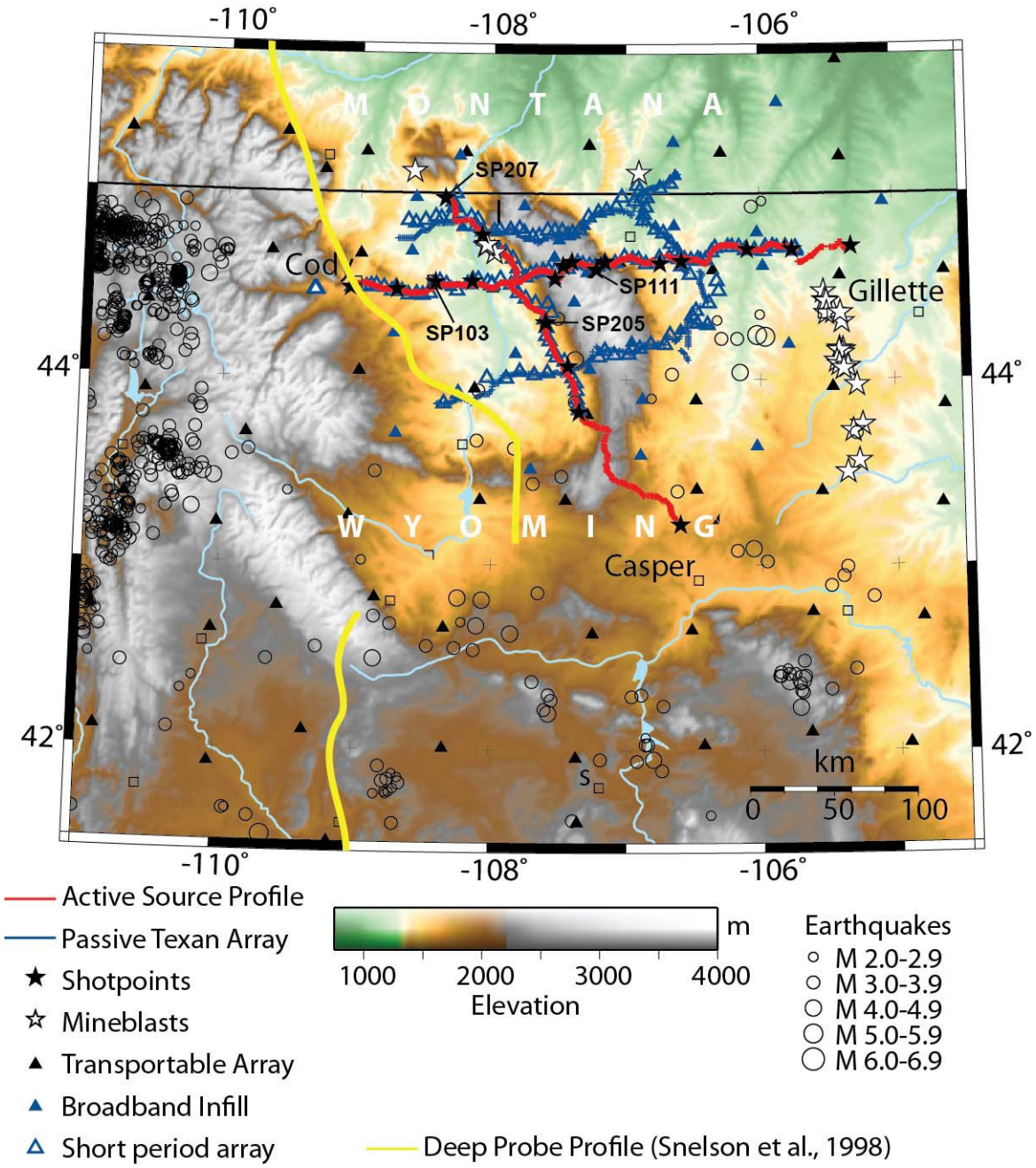

Figure 1. Regional Map showing Bighorn Arch Seismic Experiment

2. A preliminary event identification study using earthquakes, single-charge chemical explosions from the active-source profiles, and mining explosions recorded at local to near-regional distances. Figure 2 shows event locations and types.

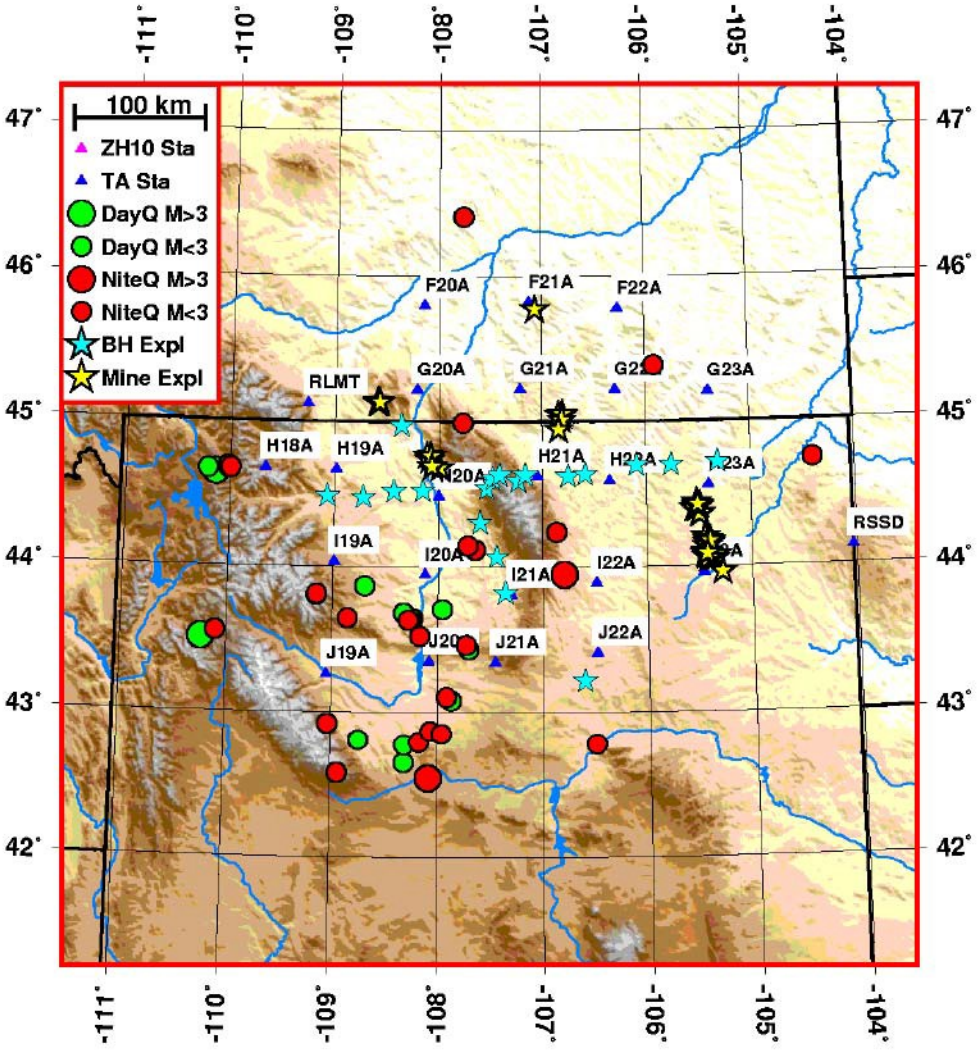

Figure 2. Stations and events used for discrimination study.

2. BACKGROUND

Basement-involved foreland arches, such as the Bighorn Arch in north-central Wyoming, are typical of Laramide orogenesis in the central Rocky Mountains. However, the mode of arch shortening at depth remains unresolved due to lack of geophysical imaging. Current hypotheses for lithospheric geometries and kinematics across the Bighorn Arch each predict distinctly different lower crustal deformation patterns and Moho topography. These different hypotheses include (Figure 3): domino-like lithospheric fault blocks [1], crustal detachment and buckling [2],[3], lithospheric buckling [4], and pure-shear thickening [5], [6].

BASE was designed to image lower crustal and upper mantle structure in order to test various hypotheses for shortening across the Bighorn Arch. The active-source seismic experiment was specifically designed to constrain Moho depths and geometry across the study region and to identify mid-crustal layers and detachment surfaces associated with arch formation.

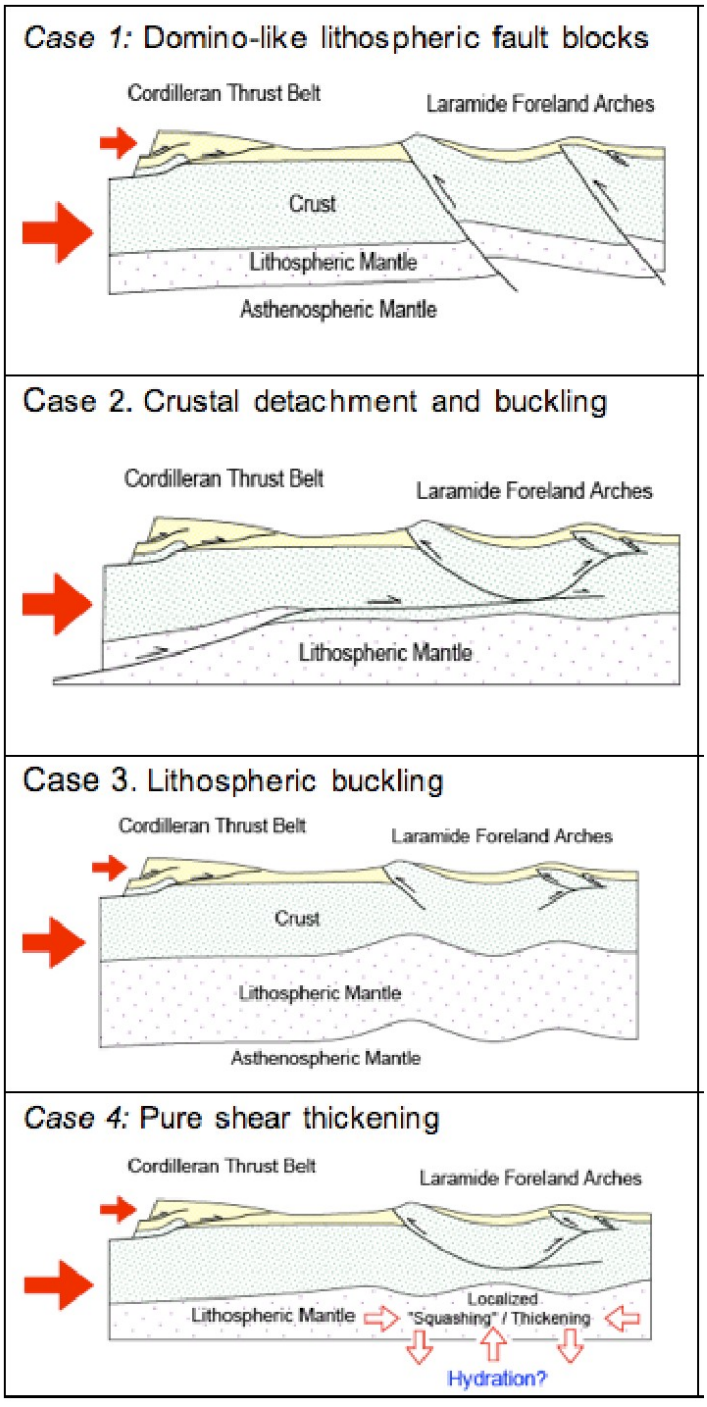

Figure 3. Tectonic models for basement-cored arch formation.

Various discrimination studies have been designed to quantify the differences between mining explosions and earthquakes in the northern Wyoming and southern Montana region given the abundance of mining activity in the area. In preparation for the work presented here, we used the following discriminants to test event identification ability in the broader region in 2009: time-of-

day, time-frequency, and amplitude ratios. Figure 4 shows earthquakes (yellow circles), explosions (red stars), and regional seismic stations (blue triangles) used in this initial study. The red outline shows the extent of the Powder River Basin and the blue lines illustrate distinct geologic provinces. Note the sparse station spacing used in these preliminary studies compared to the station spacing in the BASE deployment (Figure 1).

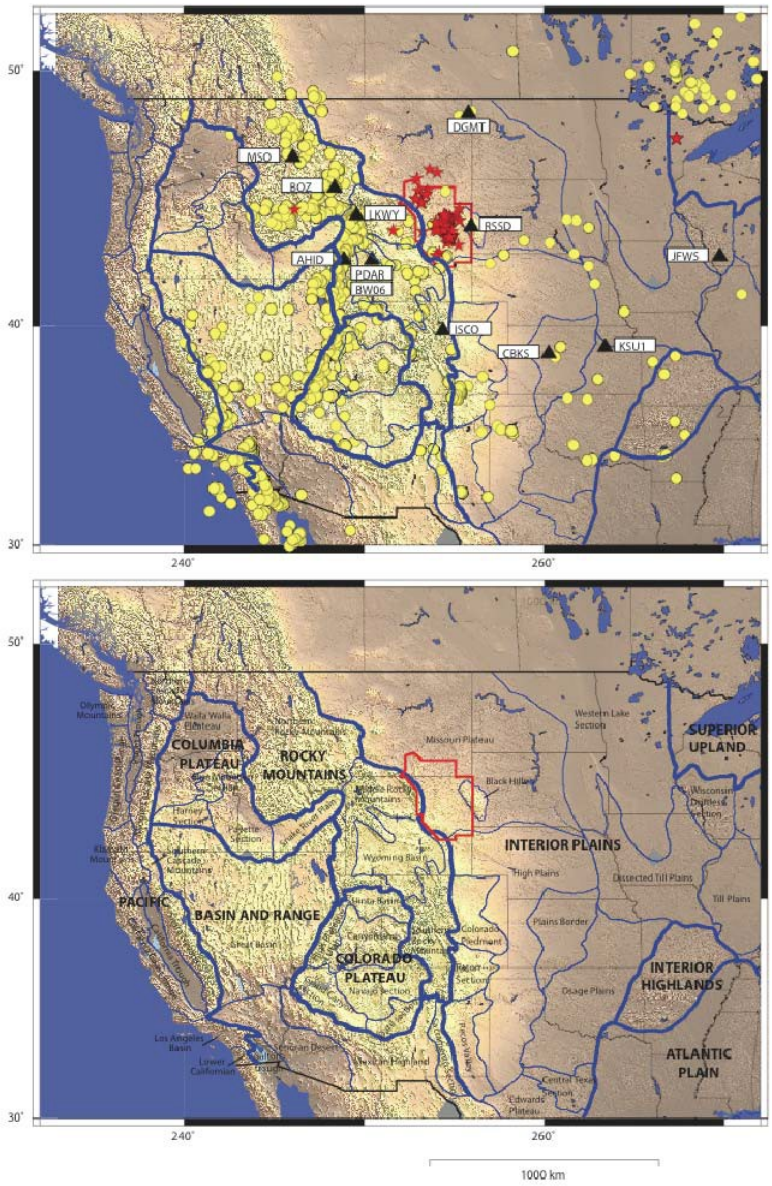

Figure 4. Regional events and stations used in preliminary study.

The time-of-day discriminant [7], [8], was used to verify the catalog consistency and evaluate general trends of the region. The time-frequency discriminant helps identify delayed-fired sequences common in mining regions and separates the largest mining events from background seismicity [9], [10]. Figure 5 shows results from time-frequency discrimination for eight stations in the western US. The amplitude ratio discriminant [11], [12], [13], was used to separate single-fired explosions from earthquakes. Figure 6 shows results from Pg/Lg (6-8 Hz) amplitude ratios

at eight stations in the western US. Comparison of event separation at different stations shows that this discriminant is strongly path-dependent, indicating a need for dense spatial sampling of the wave-field in tectonically complex regions.

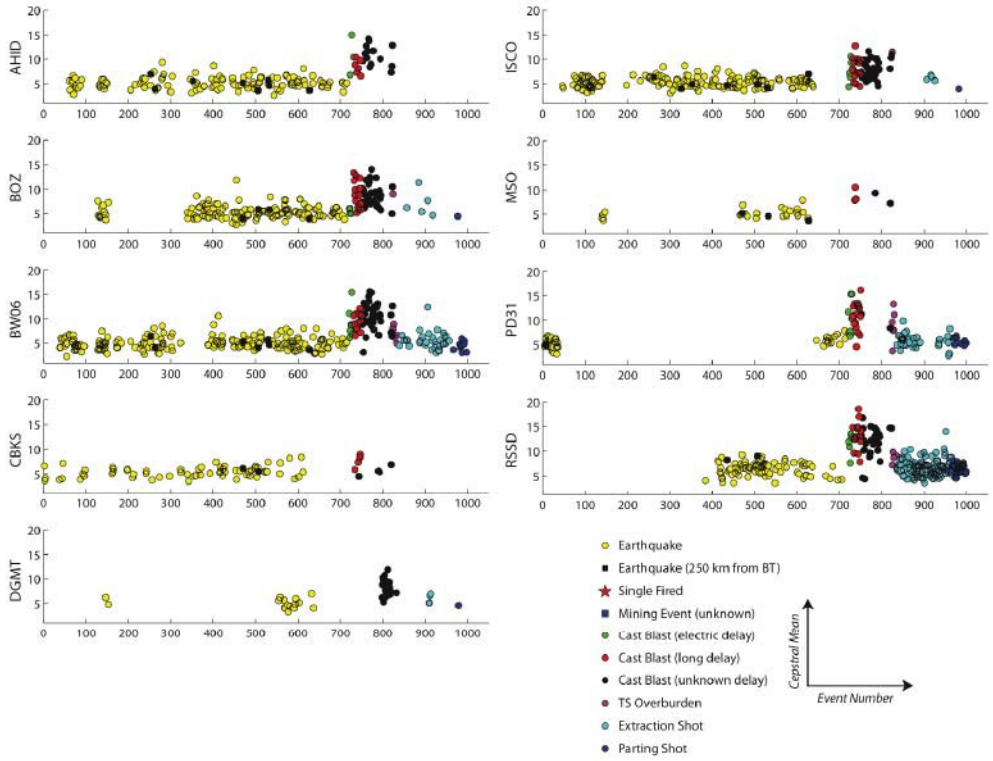

Figure 5. Time-frequency preliminary discrimination results.

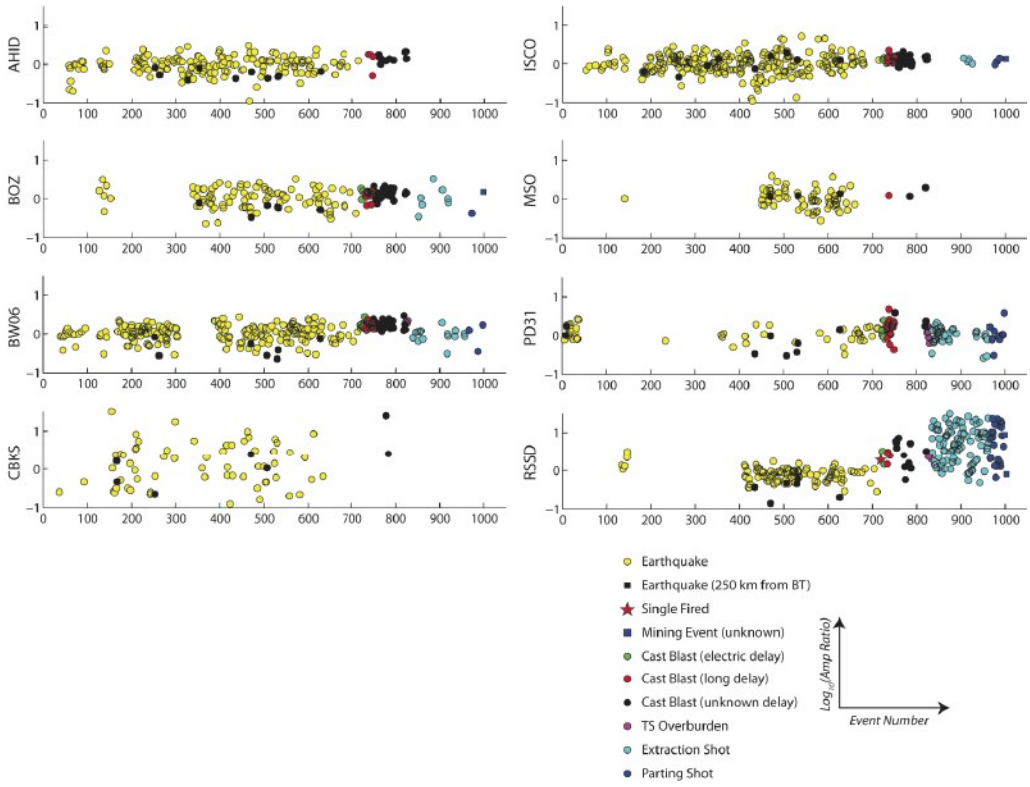

Figure 6. Pg/Lg amplitude preliminary discrimination results.

3. METHODS, ASSUMPTIONS, AND PROCEDURES

3.1 Active Source Experiment and Tomographic Analysis

The active source component of BASE consisted of two profiles. BASE01 extended ~300 km west to east (Figure 1), crossing the Bighorn Basin, the Bighorn Arch and the Powder River Basin. Data for this profile was recorded by ~1300 Reftek RT125 (Texan) seismographs with vertical-component 4.5 Hz geophones deployed at 500 m spacing within the basins. For a 100 km-long section in the mountains, receiver interval spacing along the profile was decreased to 100 m in order to improve imaging of near-vertical incidence arrivals. BASE02 traveled north to south (Figure 1), sub-parallel to the arch, for ~250 km on the western flank of the Bighorn Mountains. This profile included ~500 Texans deployed at 500 m spacing. Data from 21 single-fired shots, ranging in size between 500-2000 lbs., were recorded by the Texans across both profiles, contributing to three-dimensional coverage across the region. For this paper, we restrict our analysis to a two-dimensional inversion scheme, using data from 15 inline shots along BASE01 (Figures 7 and 8) and 6 inline shots along BASE02 (Figures 10 and 11). The dominant energy in the shots ranged between 8-20 Hz.

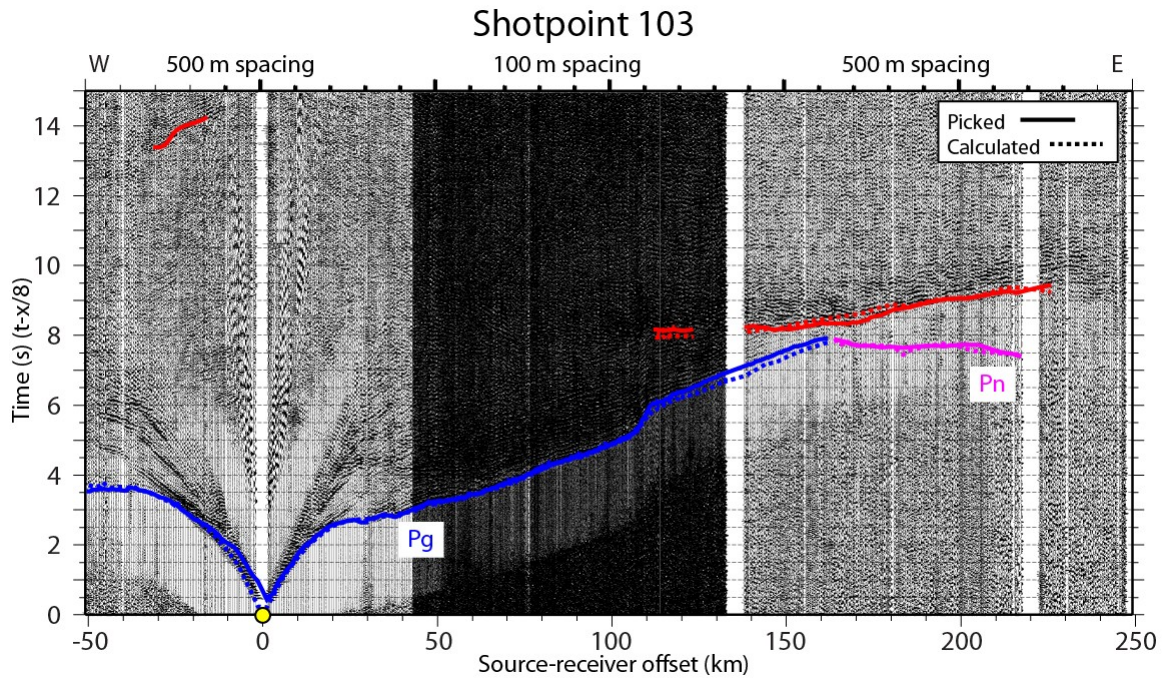

Figure 7. Shotpoint 103 data record.

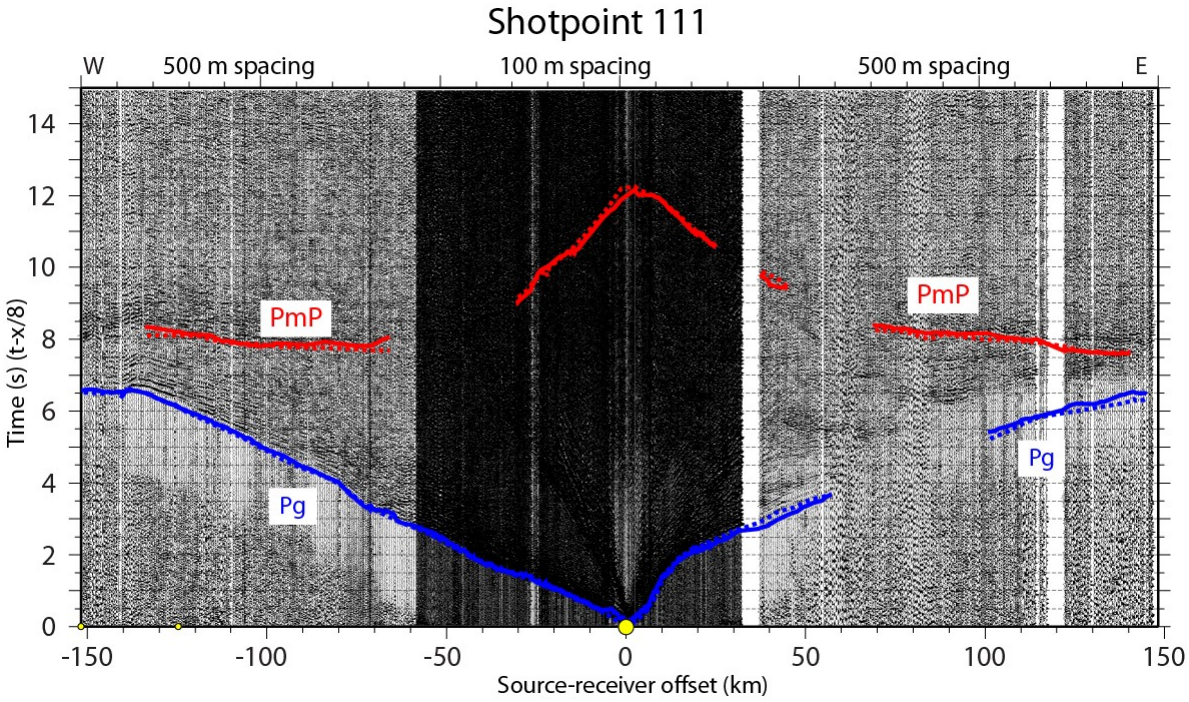

Figure 8. Shotpoint 111 data record.

For interpretation, the active source record sections were filtered between 2-18 Hz. Figures 7 and 8 show representative shot gathers from the western and central portions of the BASE01 profile with interpreted arrivals for several phases. SP 103 (Figure 7) is located at the western end of the

profile. Refracted waves traveling through the basin sediments and the crust (Pg; blue) are the first arrivals at offsets up to ~150 km. Refractions from the base of the crust (Pn; magenta) arrive first at offsets >~150 km. We also observe reflected energy from the crust-mantle boundary (PmP; red). SP111 (Figure 8) is located within the Bighorn Arch. Refracted waves traveling through basin sediments and crust are shown at all offsets (Pg; blue). The dense instrument spacing of 100 m across within the Arch allowed for interpretation of near-vertical incidence Moho reflections (PmP; red). The darker section in the middle of each record section denotes the portion of the profile in which we decreased instrument spacing from 500 m within the arch- bounding basins to 100 m across the Bighorn Arch. Data from 15 seismic shots across the BASE01 profile contribute > 9000 travel time picks to the inversion.

Some difficulty in the correct identification of secondary phases within the shot gathers arises for two primary reasons: complicated velocity structure within the lower crust and local, shallow structure such as near-surface faults or basin edges. To assist in the process of phase identification, we conducted a series of forward modeling tests. These models were constructed using velocities from initial first-arrival models. We raytraced through these starting models using both the shortest path method utilized by van Avendonk et al. (2004) [14] and the MacRay software program [15]. After raytracing through the models, we compared the resulting calculated and observed travel time curves to the data gathers. An important element in this analysis was making sure that our picks for these secondary phases were consistent across multiple data gathers. We adjusted our travel time picks where appropriate based on these comparisons.

Figures 9 and 10 show representative shot gathers from the southern and northern parts of the BASE02 profile with interpreted arrivals for crustal refractions (Pg; blue) and Moho reflections (PmP; red). Travel time picks are depicted by solid lines; calculated picks through the velocity model are depicted by dashed lines. SP 201 (Figure 9) is located at the southern-most extent of the profile; SP208 (Figure 10) is the northern-most shotpoint. Data from six seismic shots across the BASE02 profile contribute ~3000 travel time picks.

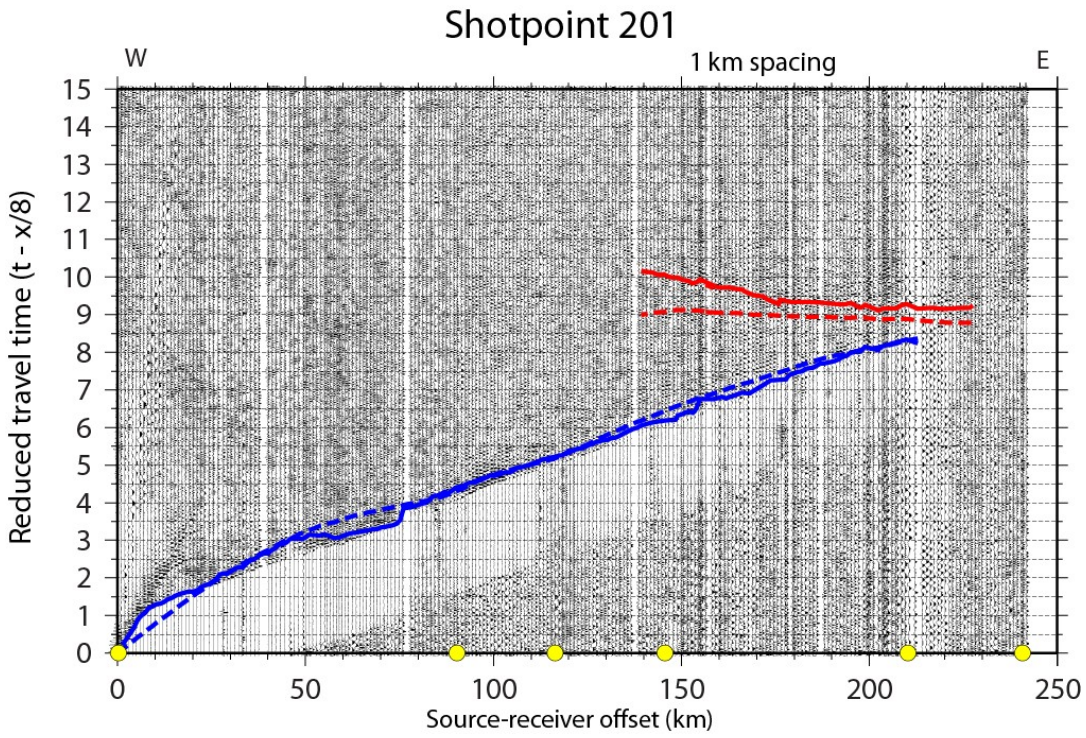

Figure 9. Shotpoint 201 data record.

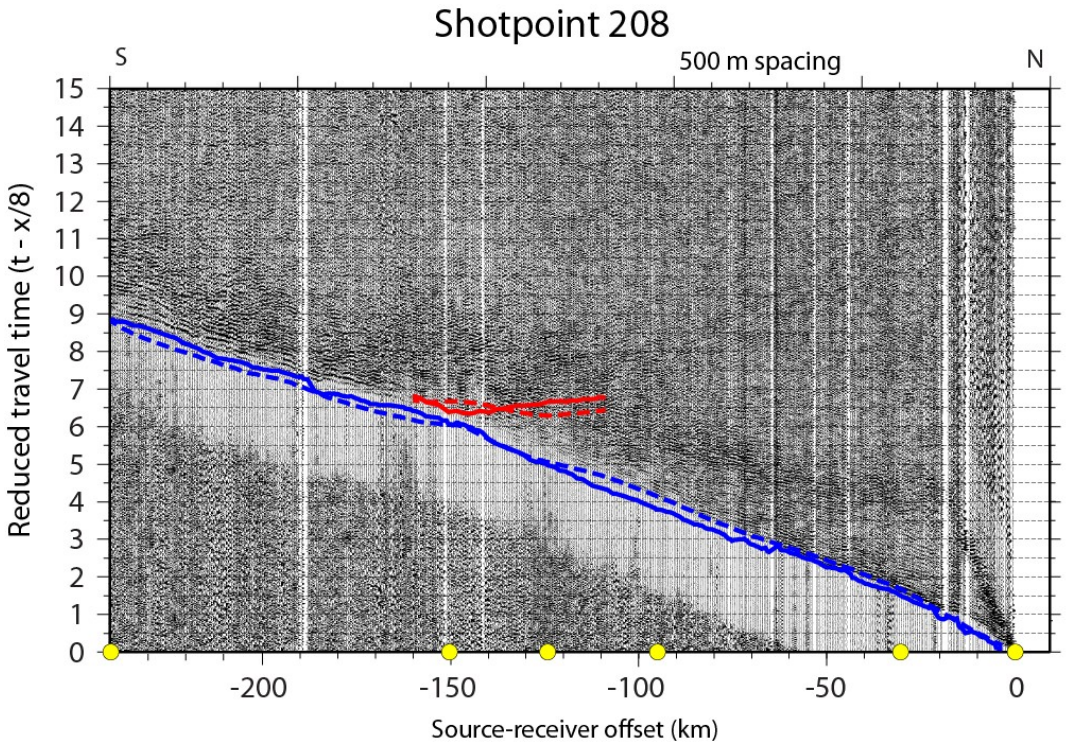

Figure 10. Shotpoint 208 data record.

By using both first-arriving and later phases from the travel time data in a joint inversion, we can simultaneously constrain seismic velocities and layer boundaries. The resulting seismic velocity models are constructed through a series of linearized tomographic inversions of travel time data following the general method of van Avendonk et al. (2004) [14]: for each iteration, we trace rays in the current velocity model using the shortest path method and ray-bending [16],[17], to develop a set of calculated raypaths and travel times. Subsequently, we invert for an update to the current velocity model using the difference between picked and calculated travel times. In each inversion, we tune the strength of smoothness constraints. The updated velocity model becomes the starting model for the next iteration of ray-tracing and inversion until a normalized data misfit, χ^2, of ~1 is achieved [14].

3.2 Discrimination Study

For our discrimination study, station and source locations are shown in Figure 2. We used data from about 20 broadband US-array stations, and station RSSD located on the edge of the Black Hills. We selected earthquakes based on event time-of-day from a region slightly broader than the BASE profile lines. Origin times are from National Earthquake Information Center (NEIC) bulletins, the Reviewed Event Bulletin (REB), and the Array Network Facility (ANF) bulletin (http://anf.ucsd.edu/). We assumed night time events (between 7 pm and 7 am local time) are earthquakes. We selected day time earthquakes from areas where a mix of night and day events occur, assuming these were areas of natural seismicity. In total, we selected about 40 earthquakes recorded from early 2009 to mid-2010. Magnitudes were not reported for many of the smaller earthquakes, but for events with reported magnitudes, sizes ranged from near 1.5 to near 4.0. Event-station distances range from a few km to nearly 500 km. See the Appendix for information on event-binning.

There are hundreds of coal mining explosions east of the Bighorn Mountains in the Powder River Basin (PRB). We selected about 50 PRB coal mining explosions where (1) we had obtained ground truth information from mine operators and (2) the events were also listed in seismic bulletins. Based on day-time event locations, we identified mining regions in the Bighorn Basin where bentonite and limestone quarrying is active, and we selected about 12 of these explosions for our discrimination analysis. Of course, we also used the ground truth events from the BASE single-charge explosions. See the Appendix for more detailed discussion of waveforms from different event types.

We measured Pg and Lg RMS amplitudes on vertical displacement seismograms over several frequency bands between 0.5 Hz and 16 Hz. See Hartse et al. (1997) [18] for a basic description of our measurement methodology. Prior to phase amplitude measurement, when no P-arrival was reported at a given station, we picked first-P on the seismogram whenever possible. For seismograms where unfavorable S/N obscured first-P, we did not make amplitude measurements. Our amplitude measurement windows ranged from 5.9 to 5.0 km/s for Pg and 3.6 to 3.0 km/s for Lg.

Following measurements of all event types, we estimated linear amplitude-distance correction parameters using earthquake data at each station, and then applied the corrections to all event types where signal amplitude exceeded pre-event noise amplitude by at least 1.75. We then

experimented with Pg and Lg spectral ratios and Pg/Lg phase ratios at each station, averaging results from all stations to generate final discrimination plots.

4. RESULTS AND DISCUSSION

4.1 Active Source Experiment and Tomographic Analysis

Figure 11 shows the 2D velocity model and ray coverage across the BASE01 profile. The root-mean-square error for the current BASE01 model is 122 ms, with a χ^2 error of 1.1. Dense ray coverage in upper 10 km of model constrains basin structure and upper crustal velocities. Modeled Moho reflections (PmP) and refractions (Pn) arrivals constrain lower crustal velocity and Moho depth beneath the Bighorn Arch and at ~80-125 km offset on either side of the Arch. Figure 12 compares travel time curves for our data picks (solid) with the calculated arrivals for crustal refractions (Pg; blue) and for the secondary arrivals, PmP (red) and Pn (magenta), through the model for the east-west profile (BASE01).

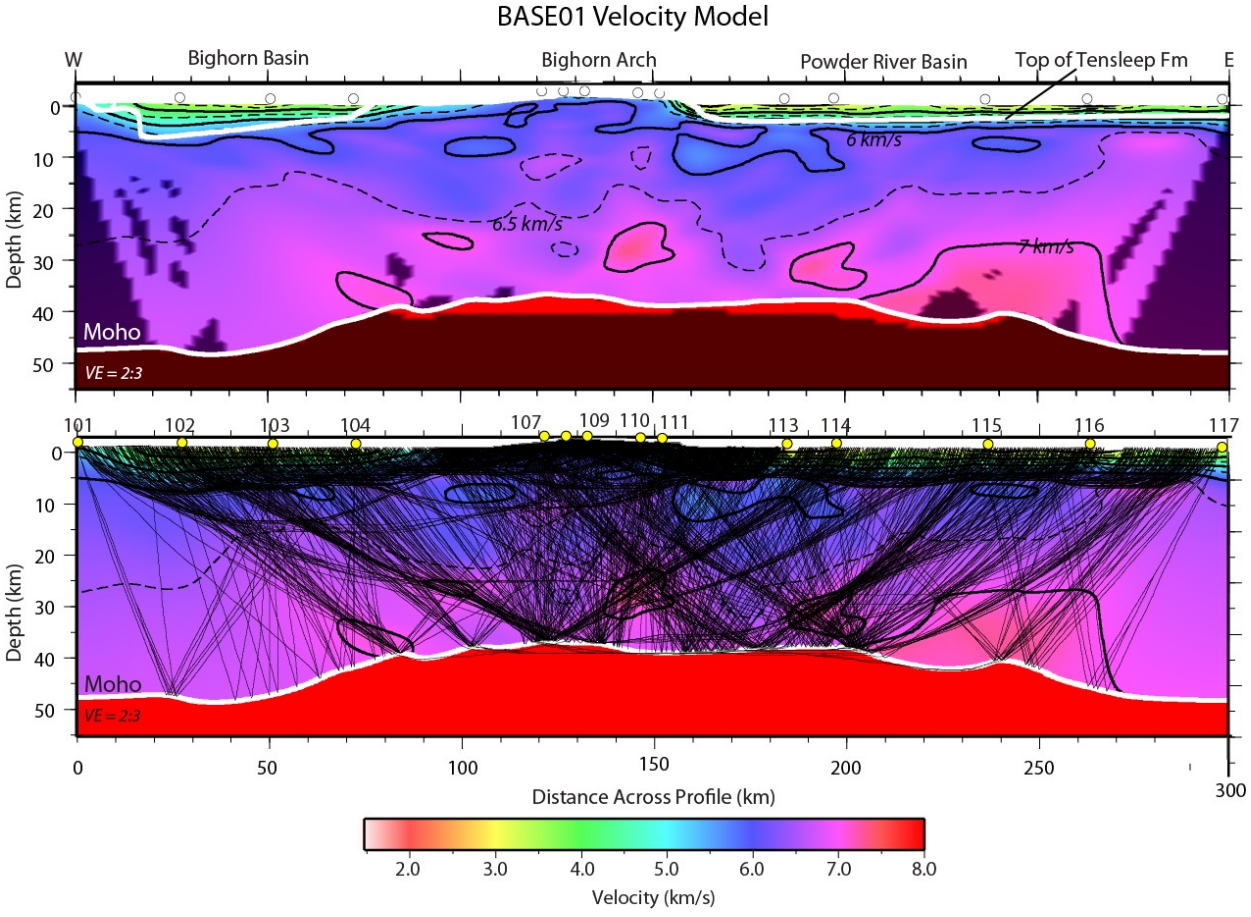

Figure 11. BASE01 velocity model.

The BASE01 velocity model includes three layers: basins, crust, and mantle. In the lower crust, the vertical velocity gradient increases slightly at ~25 km depth below the Bighorn Basin. Above

this mid-crustal transition, the profile shows thickening of the upper crust from west to east under the arch culmination. Velocities within the lower crust generally increase from west to east. The modeled Moho is relatively flat across the eastern 200 km of the profile, ranging between ~39-37 km depth. There is a slight upward deflection of ~2 km below the arch. The Moho appears to dip slightly eastward beneath the Powder River Basin, reaching a maximum depth of ~46 km (see Figure 8).

Low velocities (~2.8-4.2 km/s) in the basins on either side of the arch within the upper ~5-10 km correlate with known basin geometries. Top of Tensleep Formation (white line) approximates the top of basement [18]. The lower crust shows low-velocity zones (~5.2 km/s) within the upper 20 km that may partially coincide with known and predicted large-scale fault zones. These zones will provide targets for future kinematic modeling and reconstruction efforts.

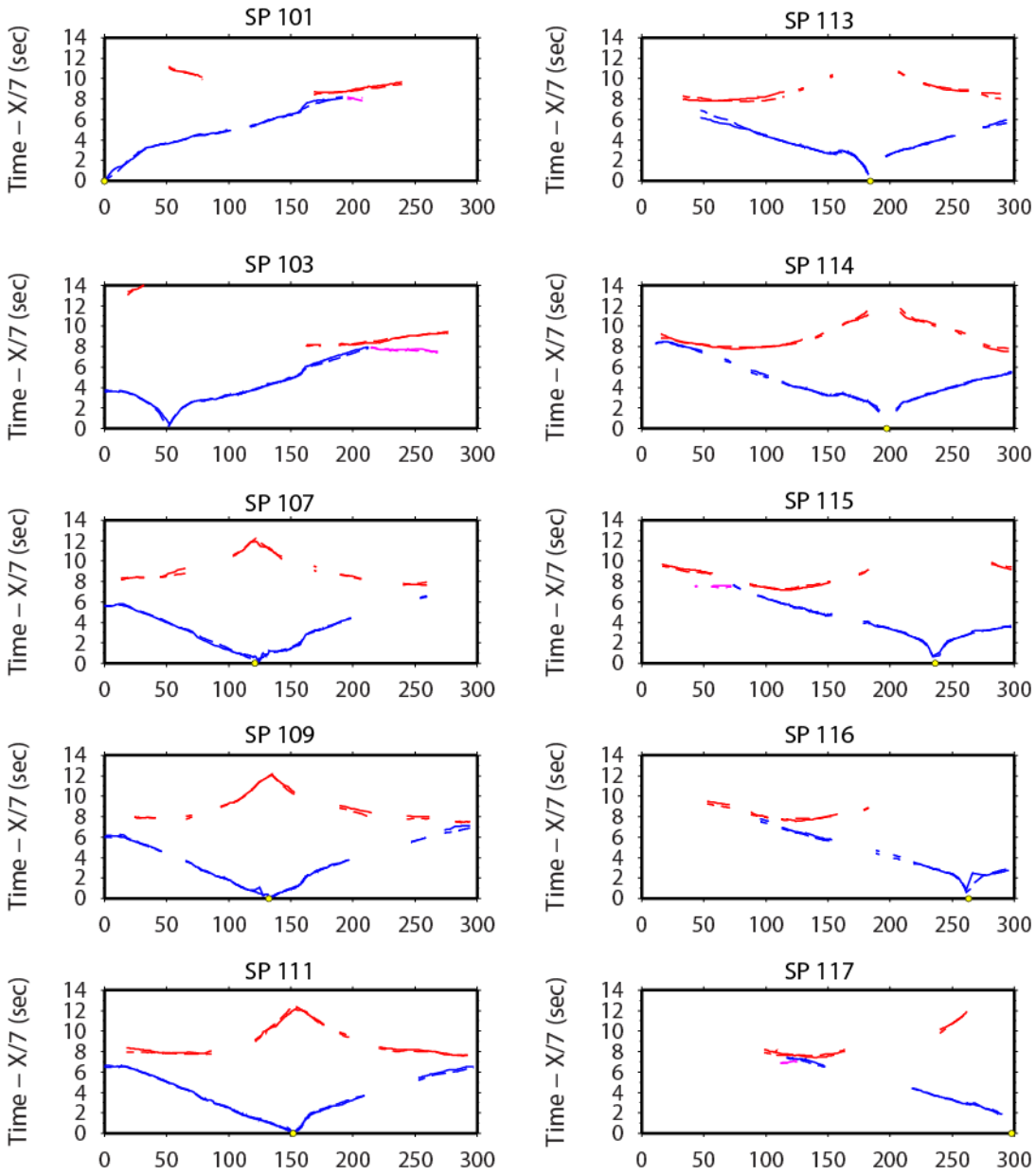

Figure 12. Data fit for BASE01 model.

Besides investigating data-misfit as shown in Figure 12, we evaluate the velocity model and determine the robustness of our interpretations by visualizing the model resolution. First, we constructed the resolution matrix from the generalized inverse that was used to create the final velocity model. The resolution matrix can then be used to predict how any seismic velocity structure will be mapped into the final model [14]. In Figure 13, we have applied the resolution matrix to test model anomalies of two different sizes to investigate the ability of our inversion to resolve seismic structure at different length scales. Resolution values are non-dimensional and range from 0 (not resolved) to 1 (fully resolved). Resolution of objects 30 km x 15 km is >0.5 in the upper ~10 km of the velocity model, and ranges between ~0.2 and ~0.7 in the deeper portions of the model (Figure 13a). Resolution of the Moho boundary is between 0.8 and 1 across the bulk of the model, with some areas of poor resolution (Figure 13a). Resolution of objects 50 km

x 25 km is >0.5 in the upper ~15 km of the model and ranges and ranges between ~0.2 and 1 in the deeper portions (Figure 13b). Resolution is especially good in the middle 100 km of the model (Figure 13b).

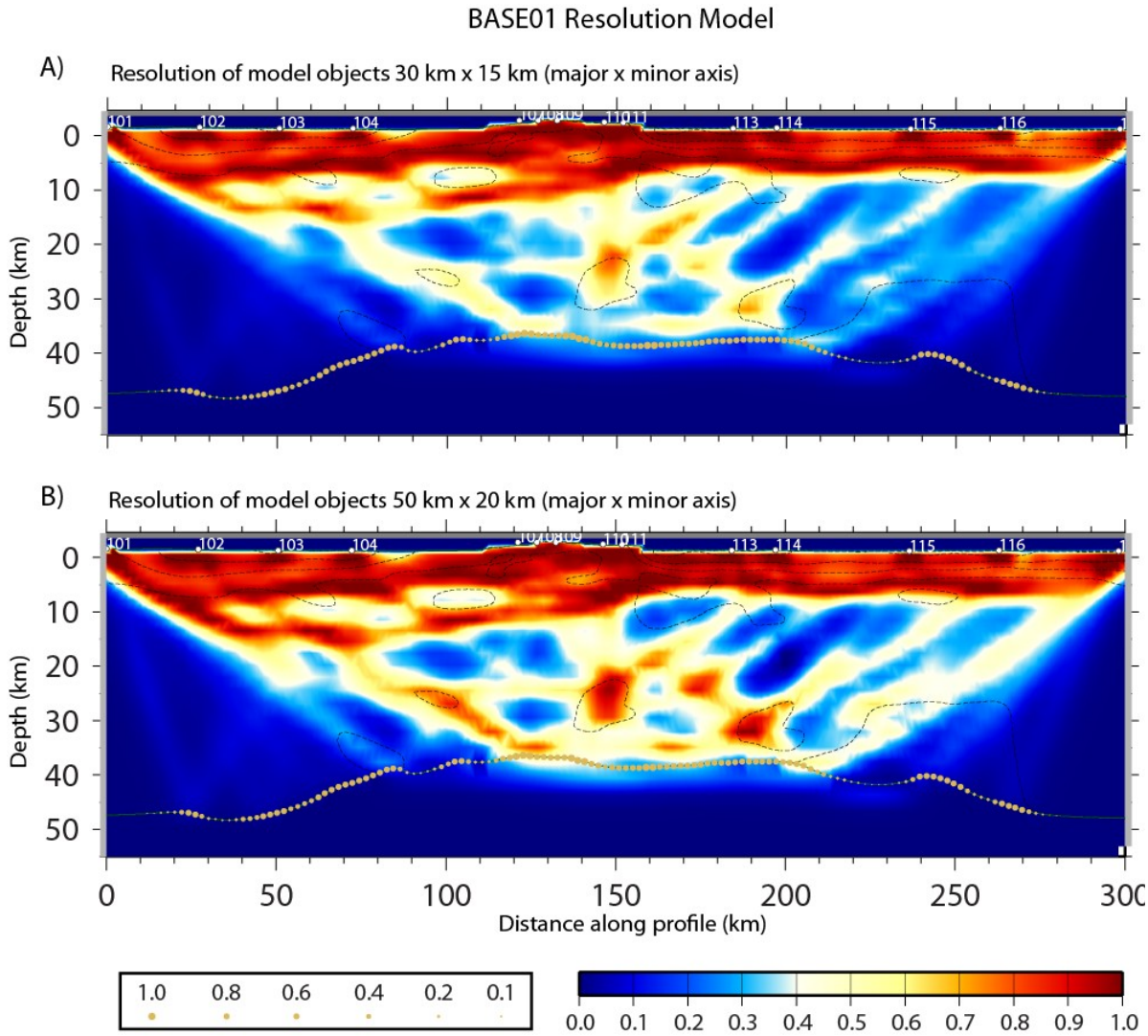

Figure 13. Resolution test for BASE01 model.

Figure 14 shows the 2D velocity model and ray coverage across the BASE02 profile. The BASE02 model has a root-mean-square error of 225 ms and a χ^2 of 2.3. Modeling across this line is currently in progress. We are continuing modeling along this profile to better fit PmP arrivals. This further modeling will likely result in a shallower Moho than what is shown here, especially in the southern portion of the line. Crustal velocities are laterally continuous in the upper crust. Figure 15 compares travel time curves for our data picks (solid) with the calculated arrivals for crustal refractions (Pg; blue) and for the secondary arrivals, PmP (red), through the model for the north-south profile (BASE02).

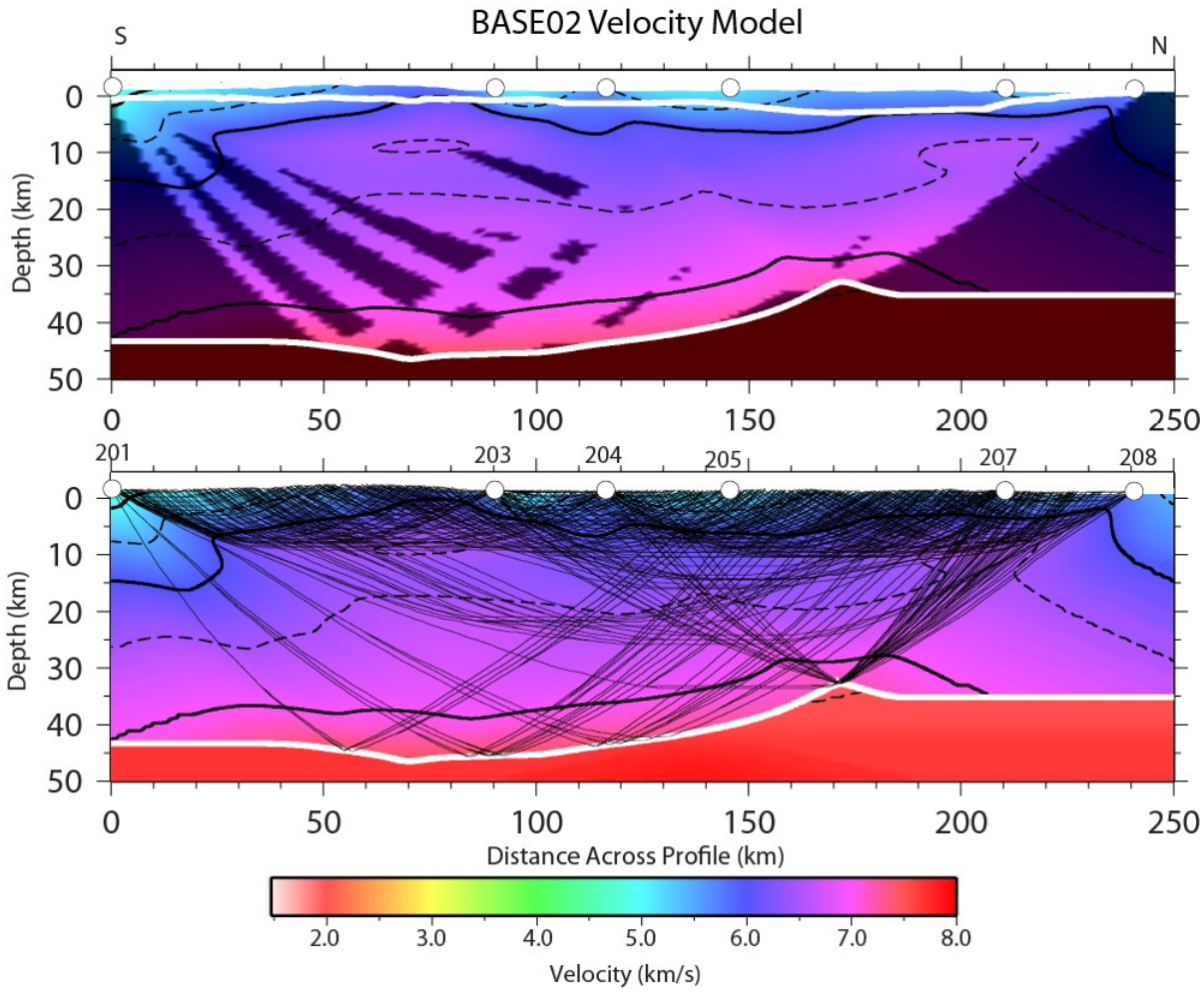

Figure 14. BASE02 velocity model.

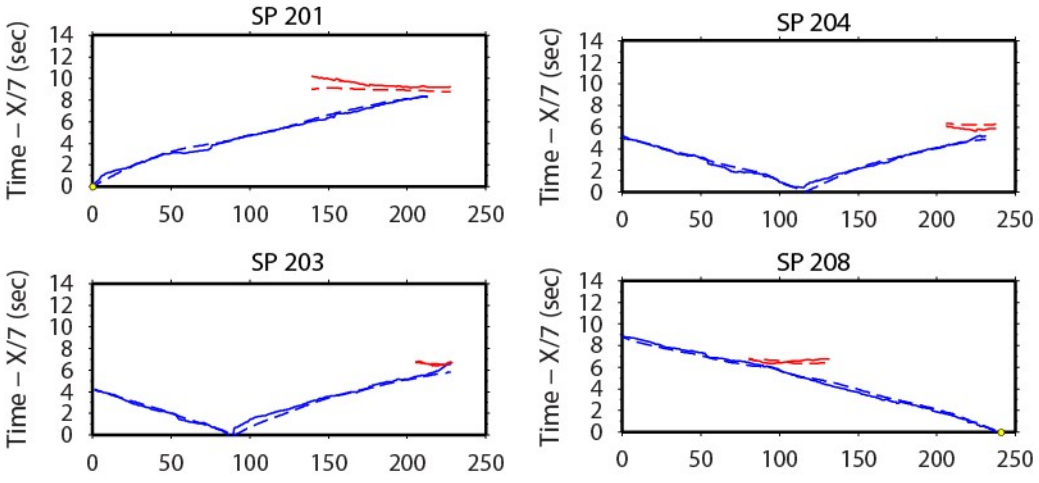

Figure 15. Data fit for BASE02 model.

An important question we can address with our current results is how crustal structure changes across the broader region of northern Wyoming. Previous investigations of crustal structure in the area include the Deep Probe seismic profile immediately to the west of our study area [19] (Figure 1). Using a combination of gravity data, well log data and seismic data from three lithospheric shots, Snelson et al. (1998) [19] calculated a crustal velocity model that features Moho depths of > 50 km and a 20 km-thick high-velocity (>7 km/s) layer at the base of the crust. Our velocity model does not extend as far west as Cody, but does give us velocity control east of Cody in the Bighorn Basin. While Moho depths compare well between the BASE model and the Deep Probe model, our lower crustal velocities show intermittent patches of >7 km/s, indicating that the 7.xx layer described by Snelson et al. (1998) [19] is discontinuous across the region.

The emerging discrepancy between the Deep Probe results and the current Bighorns model leads to some important questions regarding the regional structure of the lower crust in northern Wyoming. Namely, how does the 7.xx layer pinch out beneath the Bighorn Basin, directly east of the Deep Probe model? The degree of variability in crustal structure could ultimately prove important for discrimination of regional events. Gravity modeling across the region allows us to further investigate the changing structure of the high-velocity lower crust layer. Figure 16 shows results of gravity modeling. These models indicate that the 7.xx layer terminates beneath the Bighorn Basin. While it appears that this layer is absent beneath the Bighorn Arch itself, there is likely a high density layer beneath the Powder River Basin, outlined by the area of >7km/s lower crust on the velocity model (Figure 11). The velocity model also shows a region of high velocity upper crust at the eastern extent of the profile (Figure 11). The gravity values call for a high density body in the upper crust in this area that is collocated with a magnetic high (Figure 16).

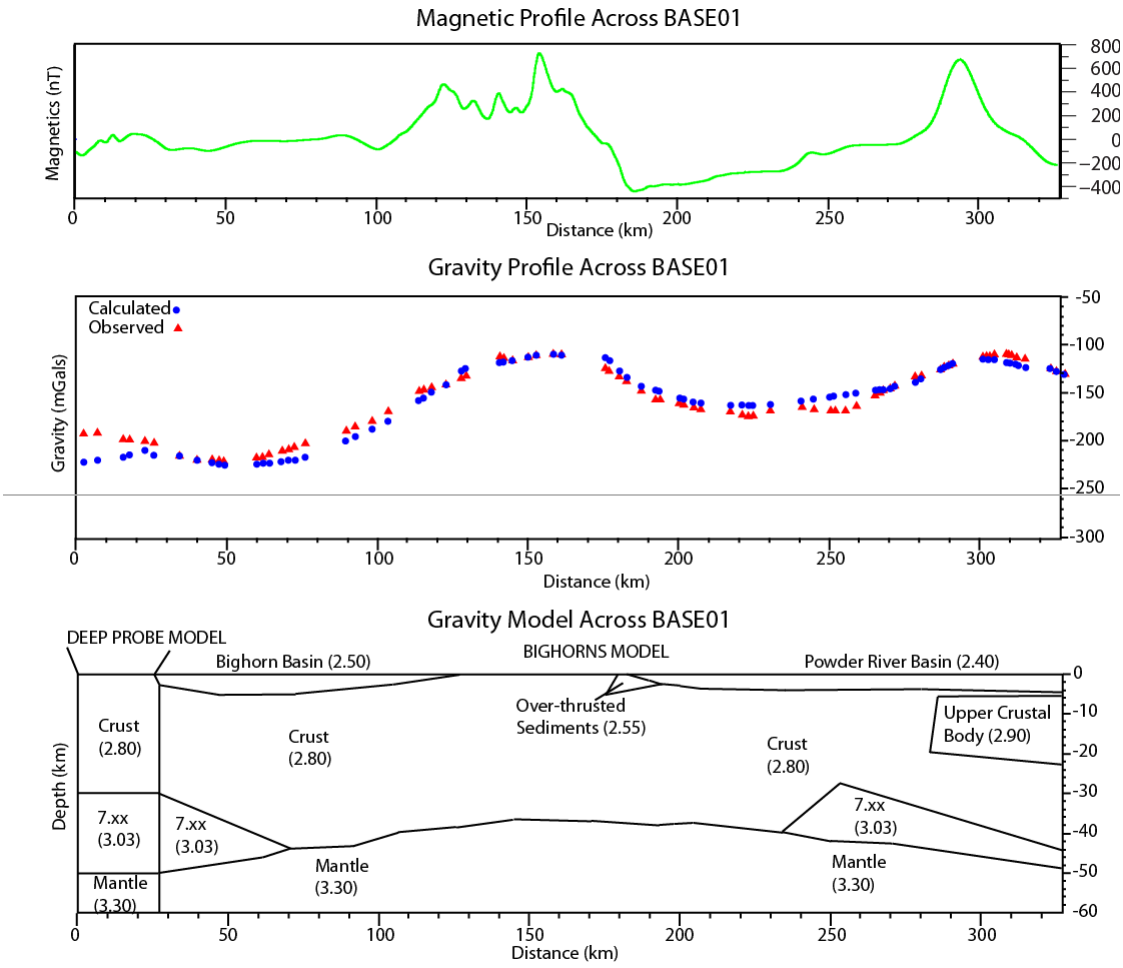

Figure 16. Gravity model across BASE01 profile.

4.2 Discrimination Study

Promising discrimination results are shown in Figures 17 and 18. The high-frequency Pg/Lg ratio (Figure 17) separates the explosions from the earthquakes. The most interesting event appears as an earthquake at the top of Figure 18, the Lg spectral ratio plot. This earthquake plots above the explosions and is almost devoid of high frequencies. This event is from Yellowstone Park, probably with a shallow focus from a geyser basin.

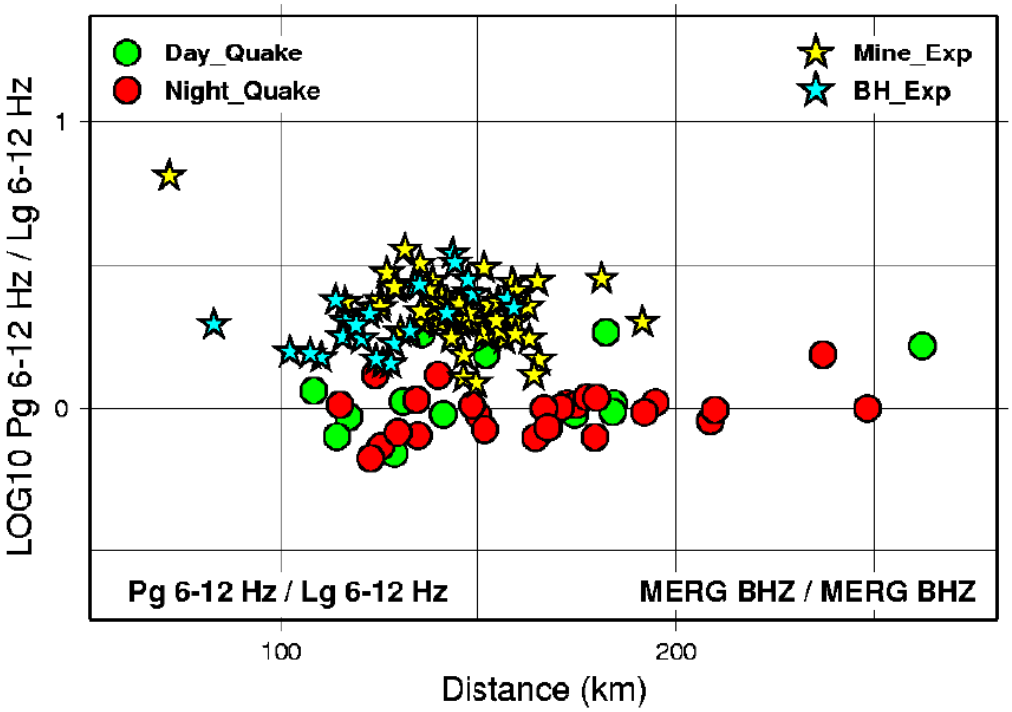

Figure 17. Pg/Lg amplitude ratio discrimination results.

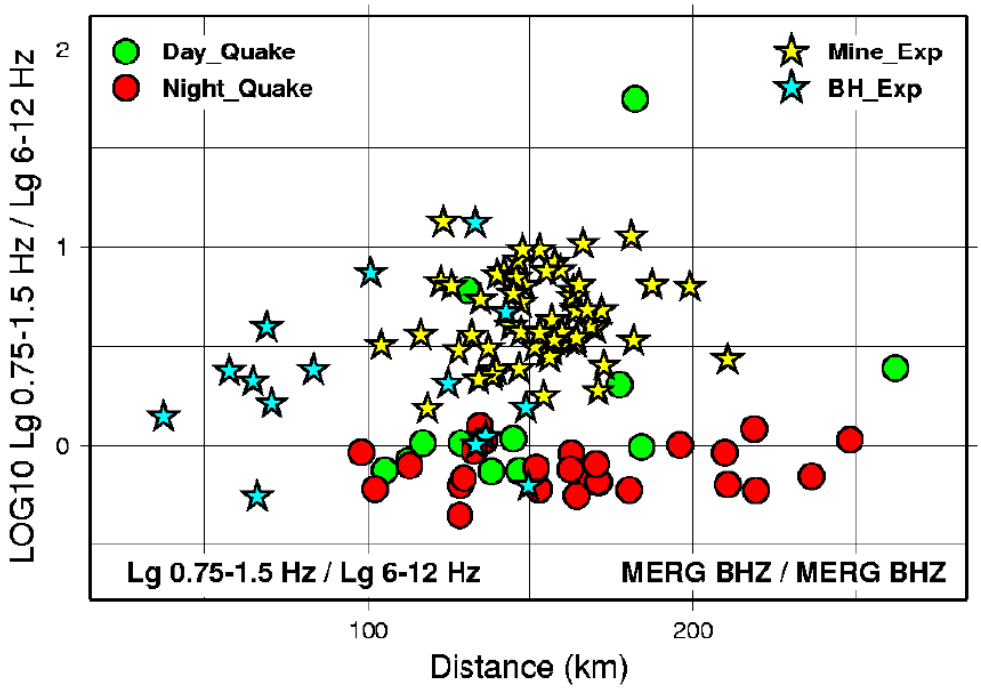

Figure 18. Lg spectral ratio discrimination results.

5. CONCLUSIONS

The tomographic results from the active source seismic experiment give constraints on crustal structure across the study area. Moho depth varies between ~37 km and ~48 km depth. The structure of the lower crust appears variable across the region with velocities reaching > 7 km/s in discontinuous patches. We also observe high velocities (>6.5 km/s) in the upper crust beneath the eastern Powder River Basin. Some low velocity patches (<6 km/s) in the upper ~10 km of the crust can be observed beneath the Bighorn Arch and immediately to the east of the Arch. The Bighorn and Powder River Basins are well defined in the BASE01 model with velocities ranging from ~2.8 km/s to ~4.2 km/s. Detailed knowledge of the variable crustal structure across the region could be valuable for understanding path effects in future discrimination efforts in the region.

For event identification, we can separate explosions from earthquakes, but we have not found a reliable method to separate the single-charge BASE explosions from the relatively uncontained, delay-fired mining explosions. We have begun experimenting with techniques to detect and measure Rg amplitudes, and we are beginning to experiment with coda amplitudes as possible discriminants that can separate single-charge from mining explosions. We also plan to apply magnitude and distance corrections (MDAC) to our discrimination data set, but first we must estimate moment magnitudes and derive appropriate attenuation models.

REFERENCES

[1] McQueen, H.W.S., and Beaumont, C., "Mechanical models of tilted block basins," in: Price, R.A., ed., Origin and evolution of sedimentary basins and their energy and mineral resources, *Geophysical Monograph* 48, 65-71, 1989.

[2] Fletcher, R. C., "Instability of lithosphere undergoing shortening: A model for Laramide foreland structures," *Geological Society of America Abstracts with Programs* 16(83), 1984.

[3] Erslev, E. A., "Thrusts, back-thrusts, and detachment of Rocky Mountain foreland arches," in: Schmidt, C. J., Chase, R. B., and Erslev, E. A., eds., Laramide basement deformation in the Rocky Mountain foreland of the Western United States, *Geol. Soc. Am. Special Paper* 280, 339–358, 1993.

[4] Tikoff, B., and Maxson, J., "Lithospheric buckling of the Laramide foreland during Late Cretaceous and Paleogene, western United States," *Rocky Mountain Geology* 36, 13-35, 2001.

[5] Egan, S. S., and Urquhart, J. M., "Numerical modeling of lithosphere shortening: application to the Laramide orogenic province, western USA," *Tectonophysics* 221, 385-411, 1993.

[6] Kulik, D.M., and Schmidt, C.J., "Regions of overlap and styles of interaction of Cordilleran thrust belt and Rocky Mountain foreland," in Schmidt, C.J., and Perry, W.J., Jr., eds., Interaction of the Rocky Mountain foreland and the Cordilleran thrust belt, *Geological Society of America Memoir* 171, 75-98, 1989.

[7] Mackey, K. G., Fujita, K., Gounbina, L. V., Koz'min, B. M., Imaev, V. S., Imaeva, L. P., Sedov, B. M., "Explosion Contamination of the Northeast Siberian Seismicity Catalog: Implications for Natural Earthquake Distributions and the Location of the Tanlu Fault in Russia," *Bull. Seism. Soc. Am*. 93, 737-746, 2003.

[8] Wiemer, S. and, Baer, M., "Mapping and Removing Quarry Blast Events from Seismicity Catalogs," *Bull. Seism. Soc. Am*. 90, 525-530, 2000.

[9] Arrowsmith, S.J., Arrowsmith, M. D., Hedlin, M. A. H., Stump, B., "Discrimination of Delay-Fired Mine Blasts in Wyoming Using an Automatic Time-Frequency Discriminant," *Bull. Seism. Soc. Am.* 96, 2368-2382, 2006.

[10] Arrowsmith, S.J., Hedlin, M. A. H., Arrowsmith, M. D., Stump, B., "Identification of Delay-Fired Mining Explosions Using Seismic Arrays: Application to the PDAR Array in Wyoming, USA," *Bull. Seism. Soc. Am.* 97, 989-1001, 2007.

[11] Bennett, T. J. and Murphy, J. R., "Analysis of seismic discrimination capabilities using regional data from Western United States events," *Bull. Seism. Soc. Am. 76*, 1069-1086, 1986.

[12] Taylor, S. R., Sherman, N. W., Denny, M. D., "Spectral discrimination between NTS explosions and Western United States earthquakes at regional distances," *Bull. Seism. Soc. Am.* 78, 1563-1579, 1988.

[13] Hartse, H.E., S.R. Taylor, W.S. Phillips, and G.E. Randall (1997), "A preliminary study of regional seismic discrimination in central Asia with emphasis on western China," *Bull. Seismol. Soc. Am.* **87**, 551–568, 1997.

[14] van Avendonk, H. J. A., Shillington, D. J., Holbrook, W. S., Hornbach, M. J., "Inferring crustal structure in the Aleutian arc from a sparse wide-angle seismic data set," *Geochem. Geophys. Geosyst.* 5, doi:10.1029/2003GC000664, 2004.

[15] Luetgert, J.H., "MacRay: Interactive two-dimensional seismic raytracing for the Macintosh," *U.S. Geological Survey Open-File Report* 92-356, 1–2, 1992.

[16] Moser, T. J., G. Nolet, and R. Snieder, "Ray bending revisited," *Bull. Seismol. Soc. Am.* 82(1), 259–288, 1992.
[17] van Avendonk, H. J. A., Harding, A.J., Orcutt, J.A., Holbrook, W.S., "Hybrid shortest path and ray bending method for traveltime and raypath calculations," *Geophysics*, 66(2), 648-653, 2001.
[18] Blackstone, D.L., "Precambrian basement map of Wyoming: Outcrop and structural configuration," in: Schmidt, C.J., Chase, R., and Erslev, E.A., eds., Laramide basement deformation in the Rocky Mountain foreland of the western United States, *Geol. Soc. Am. Special Paper*, 280 335–337, 1993.
[19] Snelson, C.M., Henstock, T.J., Keller, G.R., Miller, K.C., Levander, A., "Crustal and uppermost mantle structure along the Deep Probe seismic profile," *Rocky Mountain Geology* 33(2), 181–198, 1998.

APPENDIX

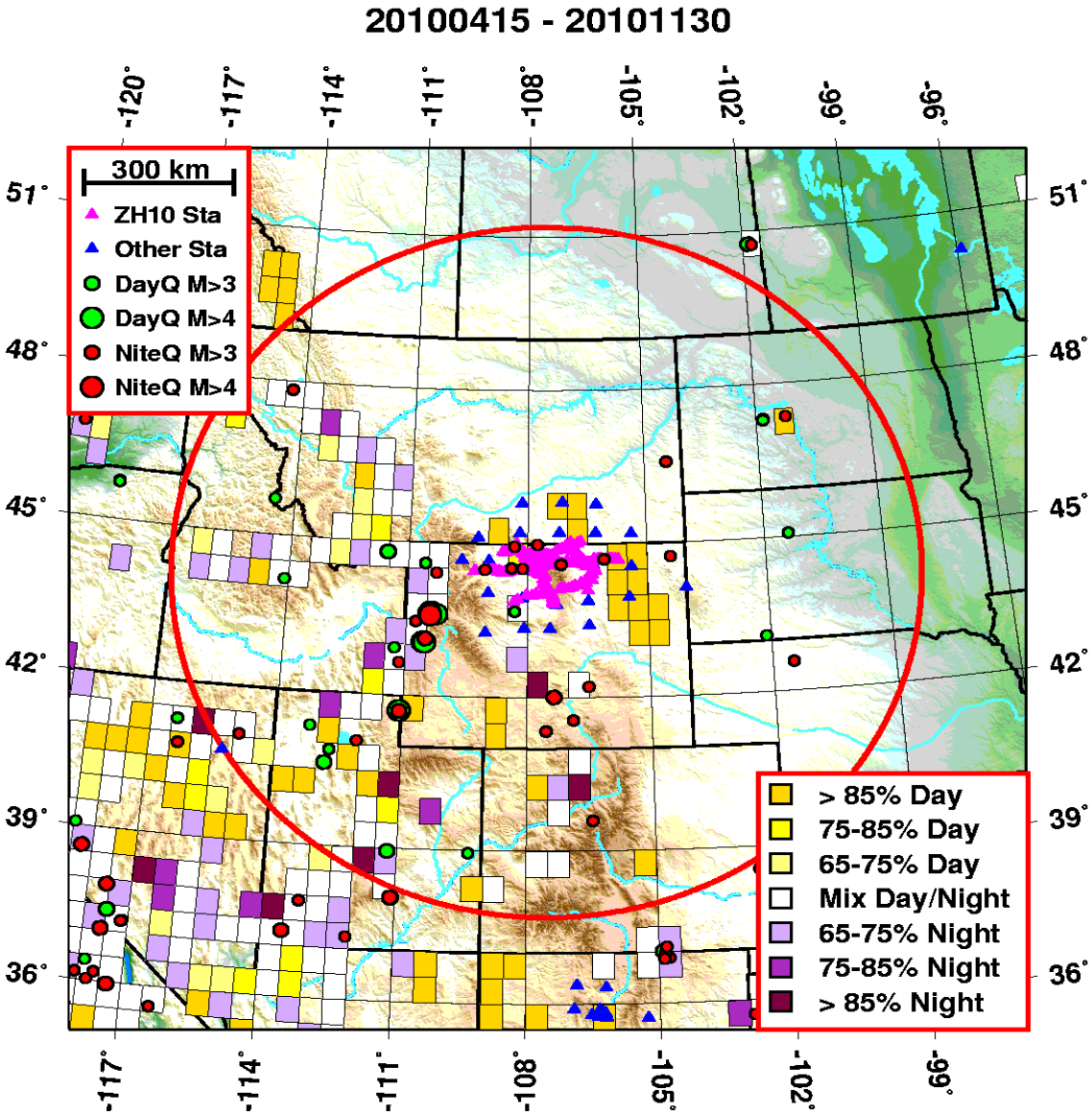

Figure 1A. Regional map of seismic stations and events used for discrimination study. Yellow and gold areas on map are dominated by seismicity reported during local day time, primarily from the US Array bulletin published at U.C. San Diego (http://anf.ucsd.edu/). Red circle is centered on the Bighorns deployment and has a 750 km radius. More discussion of earthquake and explosion selection follows in later figures.

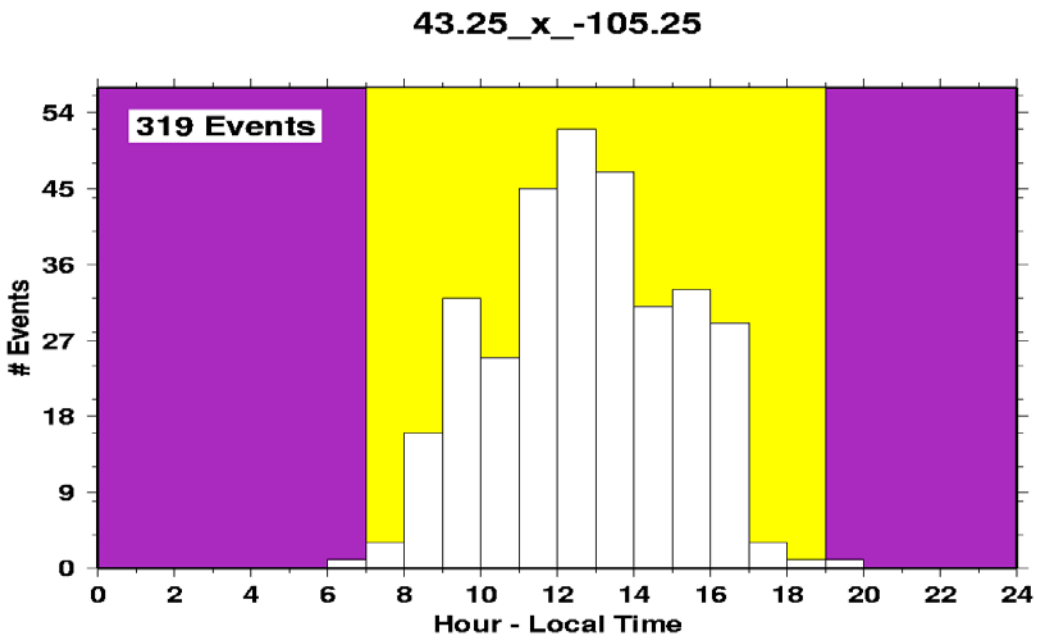

Figure 2A. Typical Powder River Basin coal mining event "bin" centered on latitude 43.25 deg N by 105.25 deg W (see Figure 1A for location). Nearly all events occur during local day time. We selected mining events for discrimination analysis from event bins such as these.

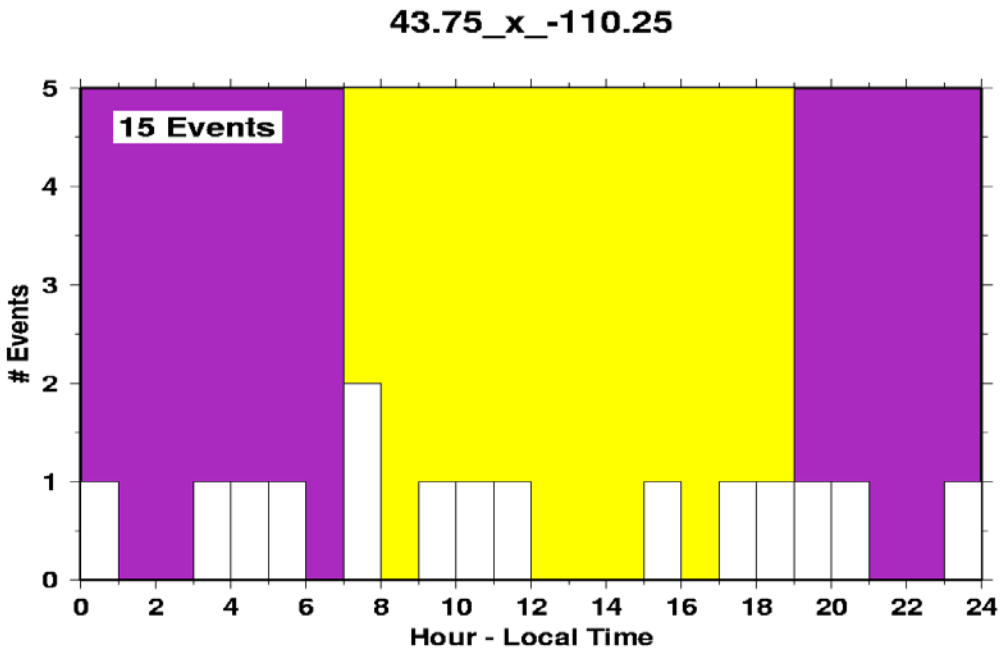

Figure 3A. A typical "white" event bin from the Yellowstone Park area of western Wyoming (see Figure 1A for location). Events occur evenly throughout local day and night time. We selected day and night earthquakes from this type of bin.

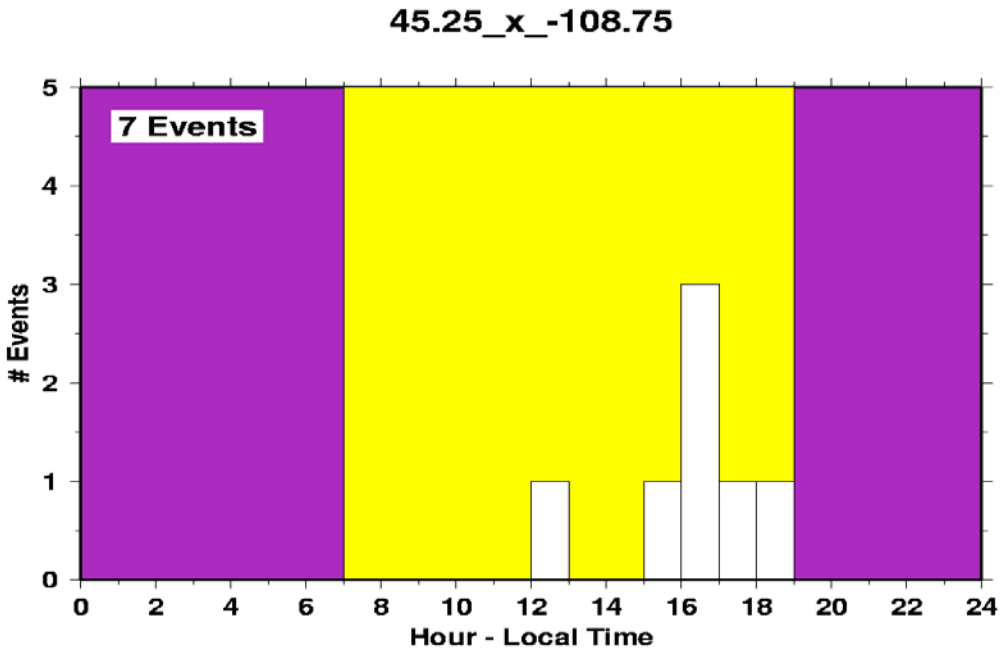

Figure 4A. We found a limestone quarry near the Bighorns Experiment explosion at shot point 208 (see Figure 1A for location), by recognizing a day time event bin and searching Google Earth imagery. We used these quarry explosions in our discrimination study.

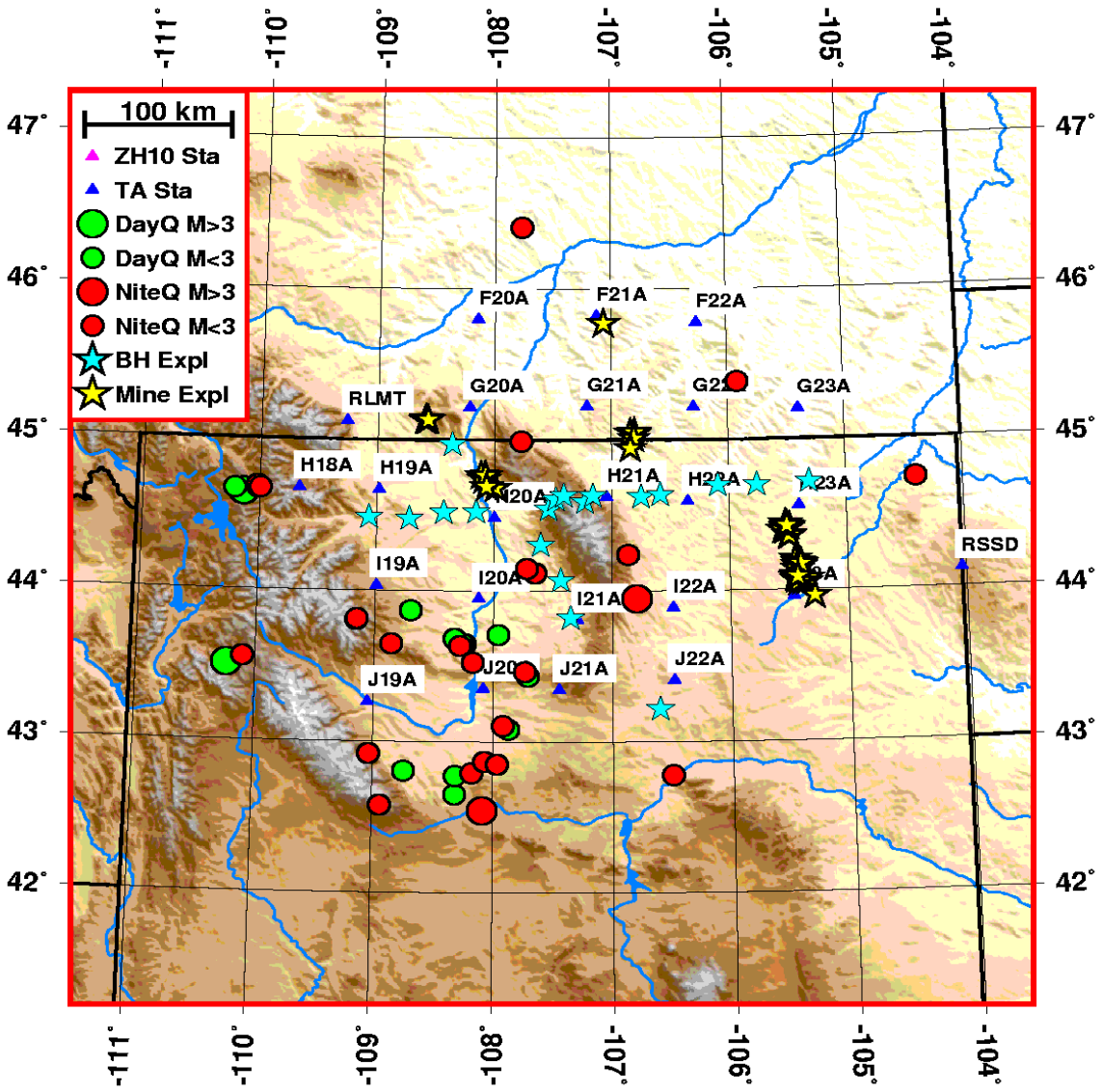

Figure 5A. Map showing events and seismic stations used for discrimination study. In total we used 60 mining explosions (mostly from Powder River Basin coal mines), 23 single-charge explosions from the Bighorns experiment, and 40 earthquakes. The blue, labeled triangles are from the U.S. Array deployment, and they were operational from August 2008 to September 2010.

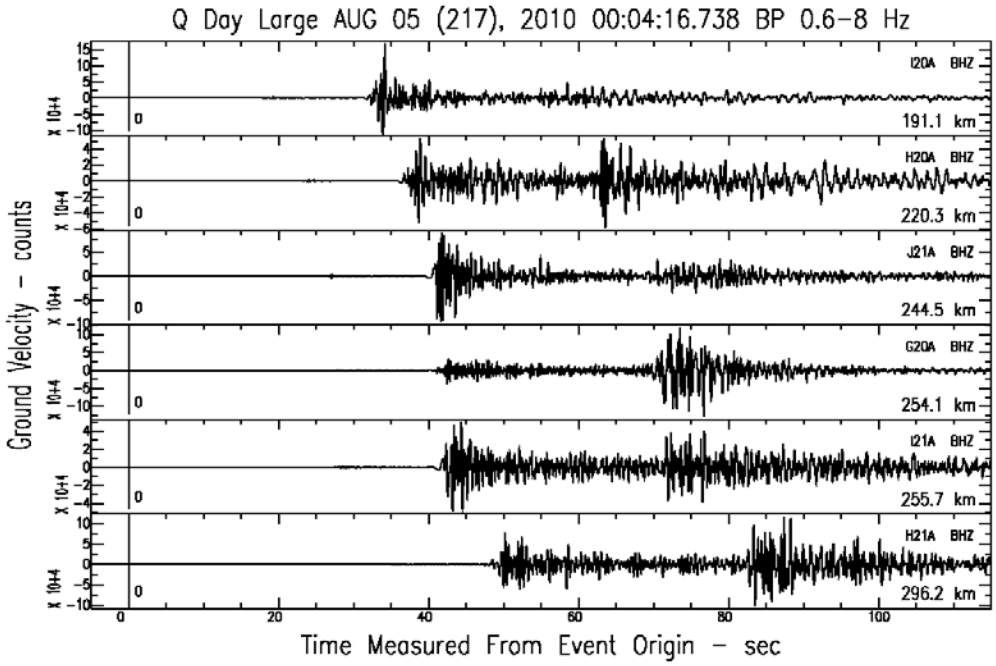

Figure 6A. Sample waveforms from a day time earthquake that occurred on the northwest end of the Wind River Mountains, near Jackson, Wyoming. Station names and event-station distances are listed on each record. Note that some records show a P-wave that is stronger than the S-wave.

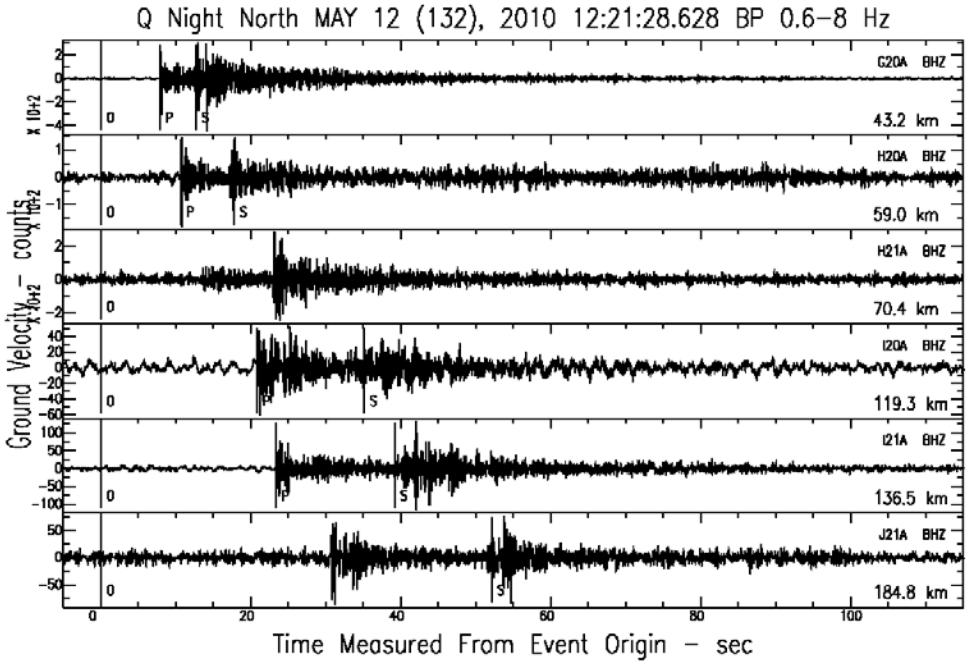

Figure 7A. Sample waveforms from a small, night time earthquake that occurred on the Montana-Wyoming border on the northeast edge of the Bighorn Mountains.

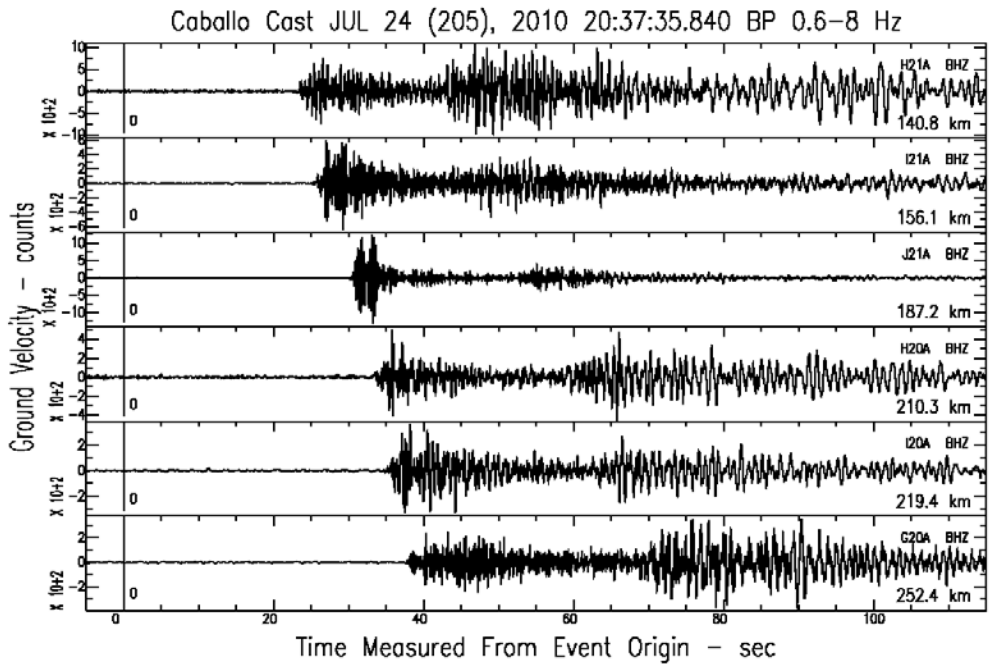

Figure 8A. Sample waveforms from a cast blast at the Caballo coal mine in the Wyoming portion of the Powder River Basin. The total weight of explosives detonated is large, but they are delay-fired.

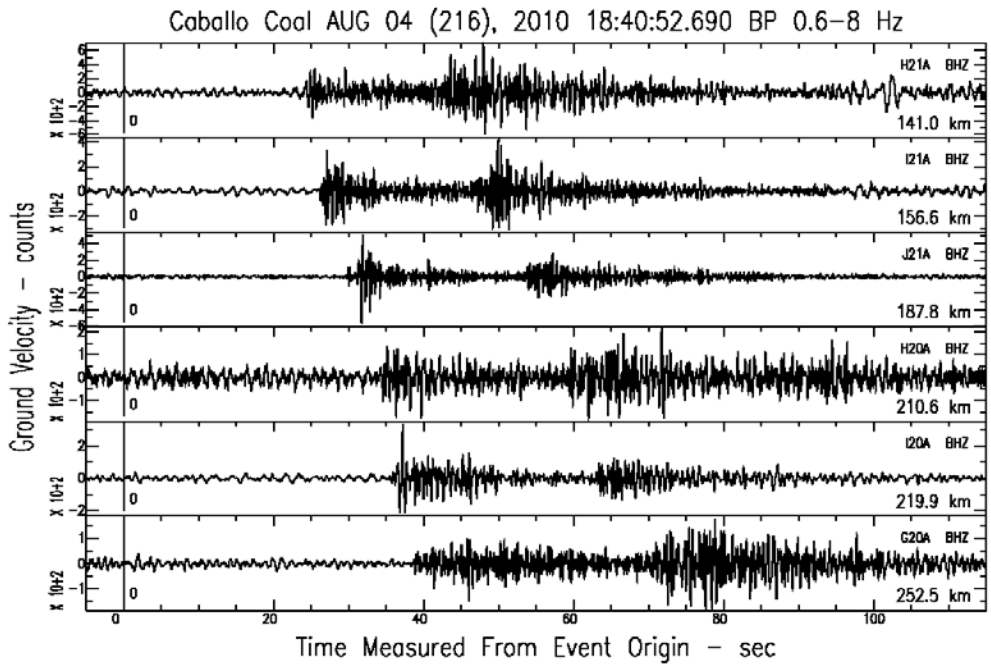

Figure 9A. Sample waveforms from a coal seam explosion at the Caballo mine in the Wyoming portion of the Powder River Basin. This is a delay-fired explosion designed to break up coal into manageable pieces. Note that signal-to-noise is not as favorable compared to the cast blast (Figure 8A), but that this coal shot appears to produce a somewhat higher-frequency signal.

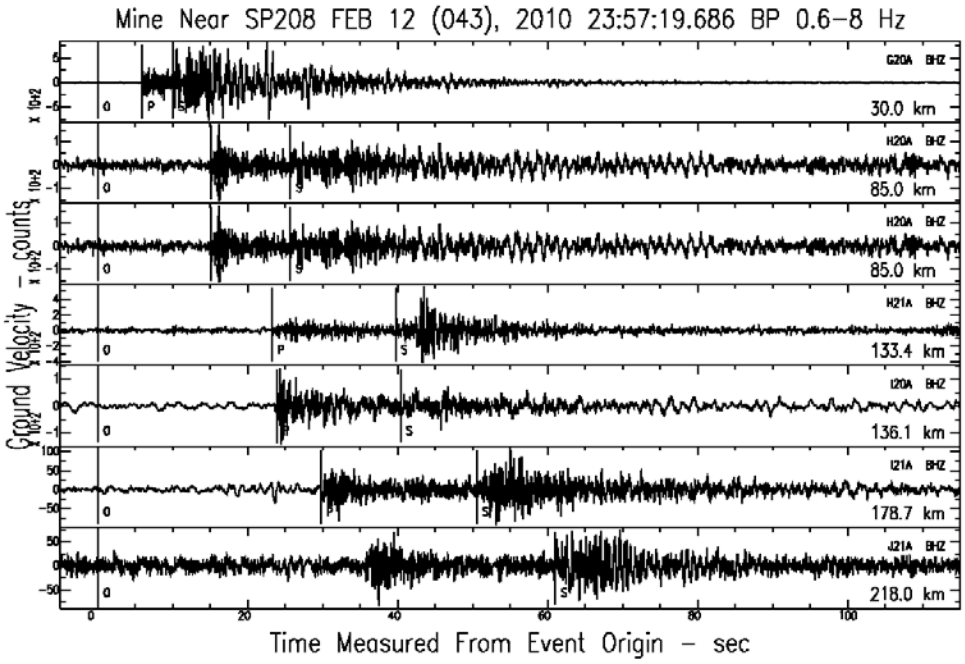

Figure 10A. Sample waveforms from a limestone quarry explosion just north of the Montana border on the west edge of the Pryor Mountains (see yellow star on Figure 5A between stations RLMT and G20A). This explosion is close to the Bighorns experiment single-charge explosion at shot point 208.

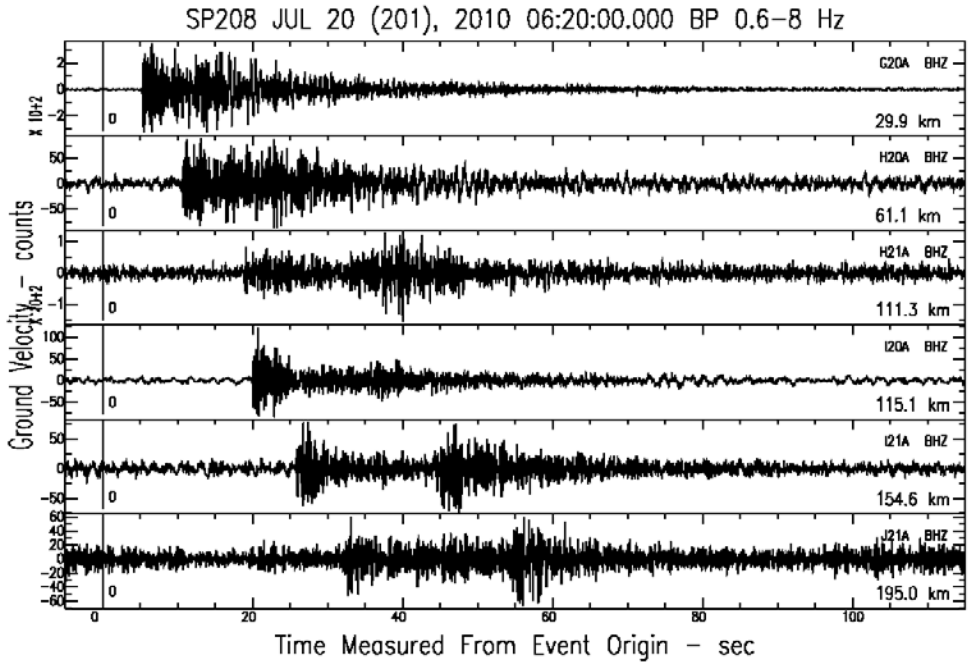

Figure 11A. Sample waveforms from the Bighorns experiment explosion at shot point 208. Explosive weight was nearly 1 ton.

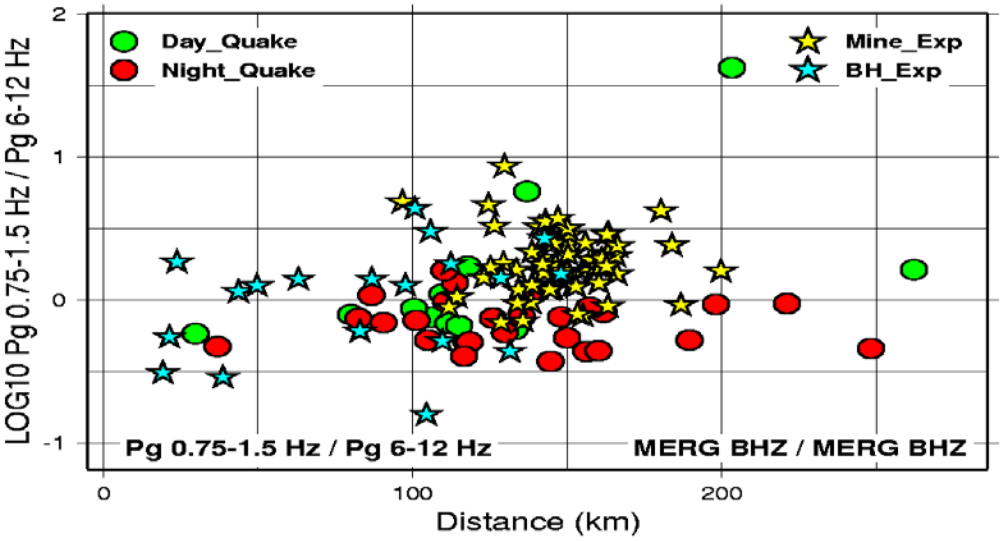

Figure 12A. Discrimination plot showing Pg spectral ratio (the 0.75-1.5 Hz band / the 6-12 Hz band) versus distance. We measured Pg and Lg phase amplitudes (RMS amplitudes on BHZ displacement records) in several frequency bands between 0.5 Hz and 12 Hz. Using earthquake results, for each seismic station, we found and removed ratio-versus-distance trends from the ratios of all event types. We then averaged results across all stations shown in Figure 5A. The distances shown here are averages of all event-station distances. A signal-to-noise test was applied to each amplitude before forming a ratio at any given station. In general, the explosions are somewhat more deficient in high frequency Pg energy than the earthquakes, but a few earthquakes plot with the explosions and a few explosions plot with the earthquakes.

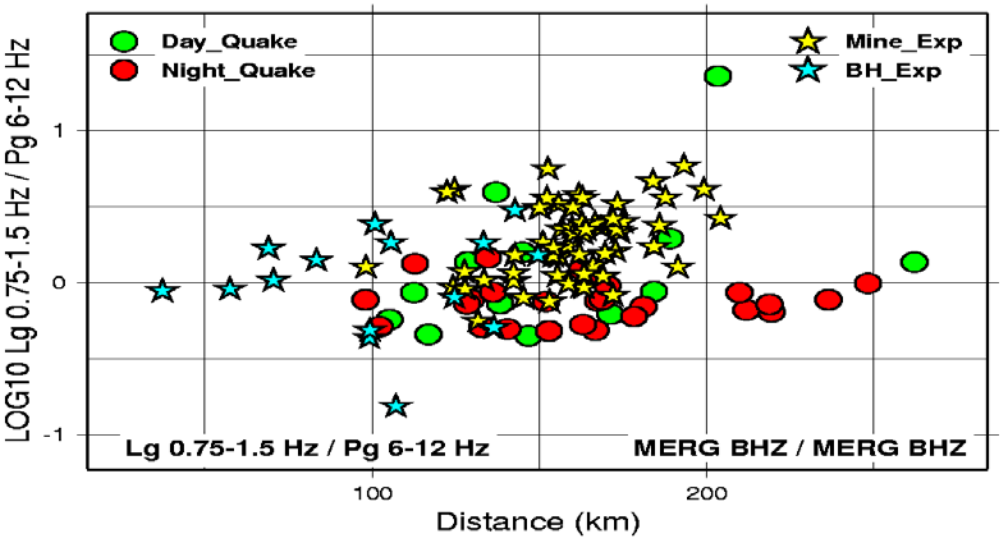

Figure 13A. Discrimination plot showing a Lg/Pg cross-spectral ratio (Lg at 0.75-1.5 Hz and Pg at 6-12 Hz) versus distance. See Figure 12A for processing information. As with the Pg spectral ratio (Figure 12A) this discriminant generally separates explosions from earthquakes, but a few earthquakes continue to plot high and merge with the explosions.

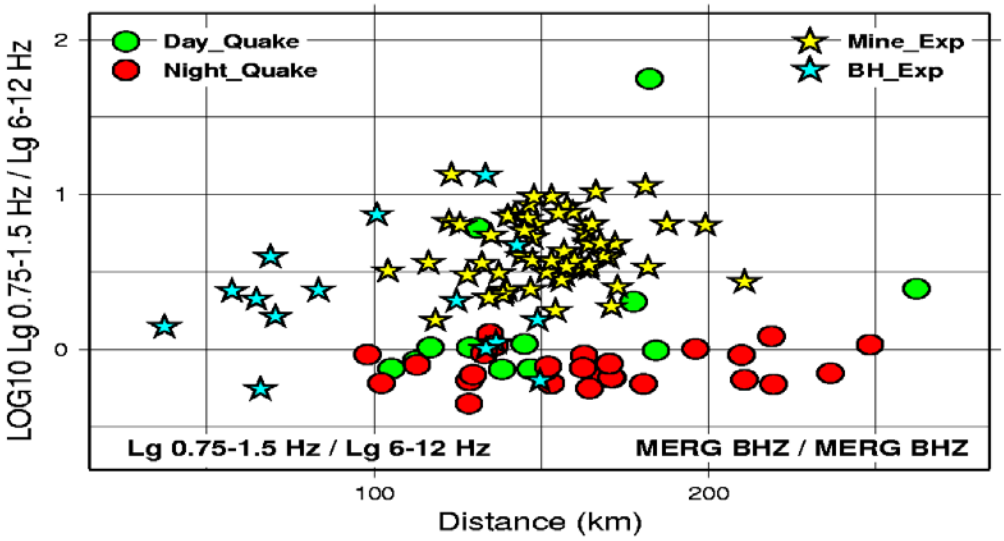

Figure 14A. Discrimination plot showing a Lg spectral ratio (0.75-1.5 Hz / 6-12 Hz bands) versus distance. See Figure 12A for processing information. Separation between explosions and earthquakes is quite good, except for a few earthquakes and a few of the Bighorns single-charge explosions.

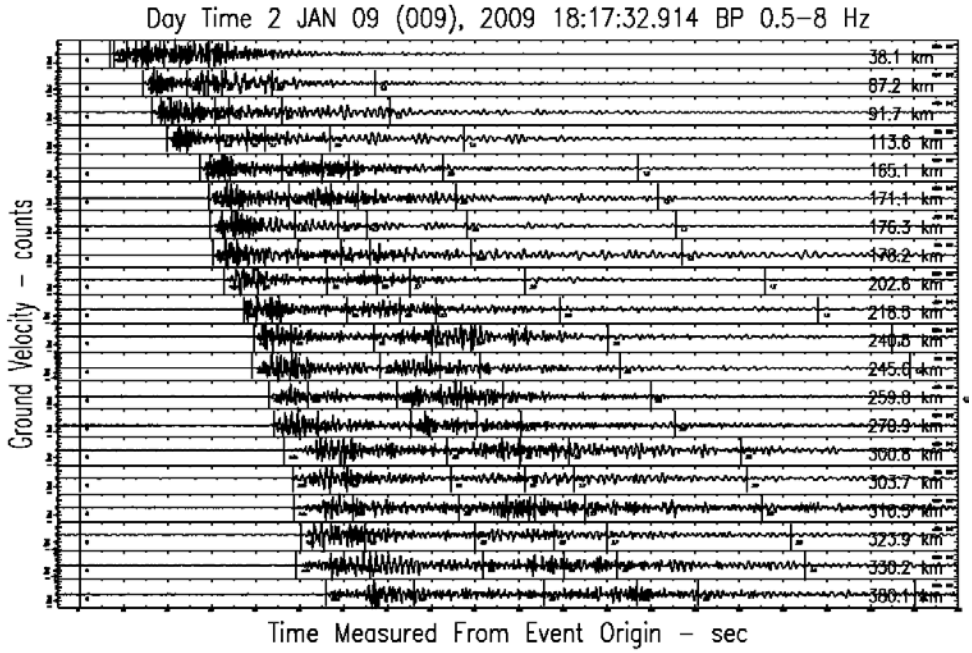

Figure 15A. A record section of the earthquake that plots above the explosions on the three discrimination plots previously shown. This is a day time earthquake from Yellowstone Park. It is dominated by low frequencies. We suspect this earthquake occurred at very shallow depth within a highly attenuating geyser basin. This earthquake requires further study.

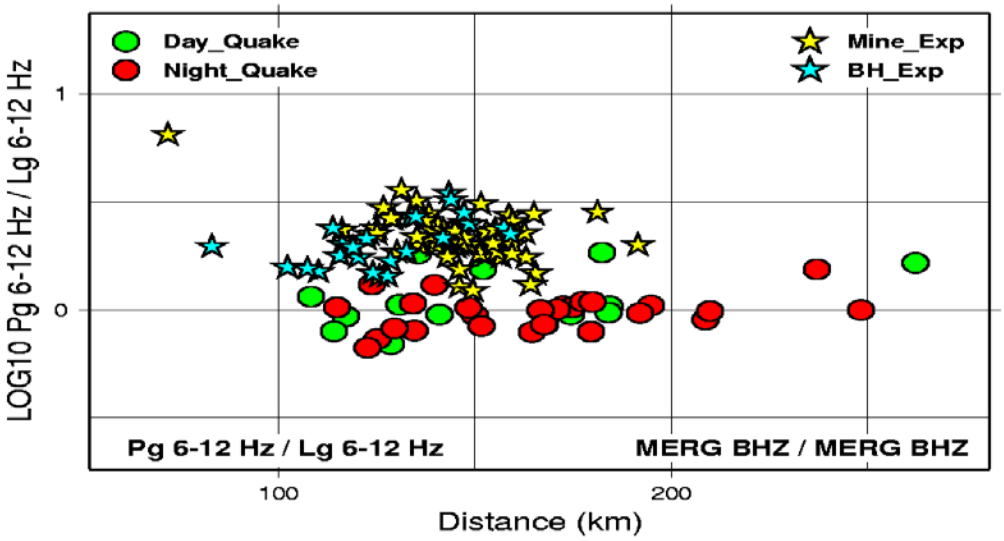

Figure 16A. Discrimination plot showing high-frequency Pg/Lg ratio results (both phases measured in the 6-12 Hz band). This is the best separation between earthquakes and explosions we obtained. The "low-frequency" Yellowstone Park earthquake is now within the explosions rather than above the explosions (at about 180 km distance). Two other day time earthquakes (at a distance of about 135 and 155 km) also plots with the explosions. Because these are day time events, we may have mistakenly classed then as earthquakes while they are actually explosions. These events needs more study.

DISTRIBUTION LIST

DTIC/OCP
8725 John J. Kingman Rd, Suite 0944
Ft Belvoir, VA 22060-6218 1 cy

AFRL/RVIL
Kirtland AFB, NM 87117-5776 2 cys

Official Record Copy
AFRL/RVBYE/Robert Raistrick 1 cy

This page is left intentionally blank.